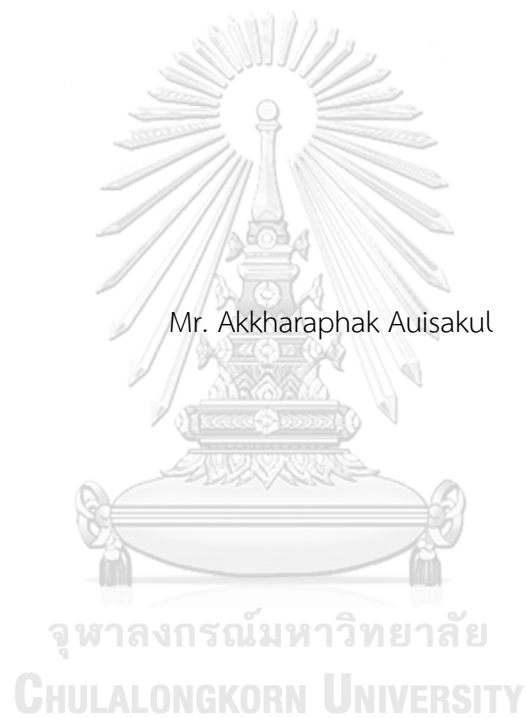


Effects of Polyaniline Thickness on Photovoltaic Properties of PANI/TiO₂ Photovoltaic
Cells



A Thesis Submitted in Partial Fulfillment of the Requirements
for the Degree of Master of Engineering in Chemical Engineering

Department of Chemical Engineering

FACULTY OF ENGINEERING

Chulalongkorn University

Academic Year 2019

Copyright of Chulalongkorn University

ผลของความหนาพอลิอะนีลีนต่อสมบัติทางไฟฟ้าของเซลล์โพลีโวลเทอิกพอลิอะนีลีน/
ไทเทเนียมไดออกไซด์



วิทยานิพนธ์นี้เป็นส่วนหนึ่งของการศึกษาตามหลักสูตรปริญญาวิศวกรรมศาสตรมหาบัณฑิต
สาขาวิชาวิศวกรรมเคมี ภาควิชาวิศวกรรมเคมี
คณะวิศวกรรมศาสตร์ จุฬาลงกรณ์มหาวิทยาลัย
ปีการศึกษา 2562
ลิขสิทธิ์ของจุฬาลงกรณ์มหาวิทยาลัย

Thesis Title Effects of Polyaniline Thickness on Photovoltaic
Properties of PANI/TiO₂ Photovoltaic Cells
By Mr. Akkharaphak Auisakul
Field of Study Chemical Engineering
Thesis Advisor Assistant Professor Palang Bumroongsakulsawat, Ph.D.

Accepted by the FACULTY OF ENGINEERING, Chulalongkorn University in
Partial Fulfillment of the Requirement for the Master of Engineering

----- Dean of the FACULTY OF
ENGINEERING
(Professor SUPOT TEACHAVORASINSKUN, D.Eng.)

THESIS COMMITTEE

----- Chairman
(Professor SARAWUT RIMDUSIT, Ph.D.)
----- Thesis Advisor
(Assistant Professor Palang Bumroongsakulsawat, Ph.D.)
----- Examiner
(Assistant Professor Paravee Vas-Umnuay, Ph.D.)
----- External Examiner
(Assistant Professor Pornchai Bumroongsri, D.Eng.)

อัครภาค อัยสกุล : ผลของความหนาพอลิอะนิลีนต่อสมบัติทางโฟโตวอลเทอิกของ
 เซลล์โฟโตวอลเทอิกพอลิอะนิลีน/ไทเทเนียมไดออกไซด์. (Effects of Polyaniline
 Thickness on Photovoltaic Properties of PANI/TiO₂ Photovoltaic Cells) อ.ที่
 ปริญญาหลัก : ผศ. ดร.พลัง บำรุงสกุลสวัสดิ์

พอลิอะนิลีนเป็นวัสดุพอลิเมอร์ราคาถูกที่มีคุณสมบัติเป็นสารกึ่งตัวนำชนิดพีที่มีความสามารถในการนำไฟฟ้าที่ดีและมีคุณสมบัติรีดอกซ์เฉพาะตัว โดยในงานวิจัยนี้ได้ทำการสังเคราะห์พอลิอะนิลีนลงบนพื้นผิวไทเทเนียมไดออกไซด์/ฟลูออไรด์ทินออกไซด์โดยตรงด้วยวิธีอิเล็กโทรพอลิเมอร์ไรเซชันในสารละลายอะนิลีนที่มีความเป็นกรดเพื่อสร้างรอยต่อพีเอ็นของพอลิอะนิลีน/ไทเทเนียมไดออกไซด์ ในการทดลองนี้ได้ทำการปรับเปลี่ยนระยะเวลาในการสังเคราะห์พอลิอะนิลีนเป็น 15 30 และ 45 นาที ที่ความหนาแน่นกระแสไฟฟ้าคงที่ 2 มิลลิแอมป์ต่อตารางเซนติเมตร เพื่อศึกษาผลของความหนาพอลิอะนิลีนที่แตกต่างกัน โดยที่ความหนาของพอลิอะนิลีนสามารถตรวจสอบได้ด้วยเทคนิคสแกนนิ่งอิเล็กตรอนไมโครสโคปและคุณสมบัติทางโฟโตวอลเทอิกของเซลล์วอลเทอิกพอลิอะนิลีน/ไทเทเนียมไดออกไซด์จะรายงานในรูปแบบค่ากระแสไฟฟ้าลัดวงจรและค่าความต่างศักย์เปิดวงจร จากผลการทดลองแสดงให้เห็นว่าระยะเวลาในการสังเคราะห์พอลิอะนิลีนที่ 30 นาที ให้ความหนาของพอลิอะนิลีนเฉลี่ยเท่ากับ 399 นาโนเมตร ซึ่งสามารถแสดงคุณสมบัติทางโฟโตวอลเทอิกได้อย่างมีนัยสำคัญ นอกจากนี้ในงานวิจัยนี้ได้ทำการสังเคราะห์ไทเทเนียมไดออกไซด์แท่งนาโนบนแผ่นไทเทเนียมในสารละลายอิเล็กโทรไลต์เบสฟลูออไรด์โดยใช้วิธีอิเล็กโทรเคมีคอลแอโนไดเซชันและปรับเปลี่ยนระยะเวลาในการสังเคราะห์ไทเทเนียมไดออกไซด์แท่งนาโนเป็น 45 และ 60 นาที ที่ความต่างศักย์คงที่ 60 โวลต์ จากผลการทดลองแสดงให้เห็นว่าระยะเวลาในการการสังเคราะห์ไทเทเนียมไดออกไซด์แท่งนาโนที่ 60 นาทีเหมาะกับการสร้างรอยต่อพีเอ็นกับพอลิอะนิลีนที่สังเคราะห์เป็นระยะเวลา 45 นาที เพื่อแสดงคุณสมบัติทางโฟโตวอลเทอิก

สาขาวิชา วิศวกรรมเคมี

ลายมือชื่อนิสิต

ปีการศึกษา 2562

ลายมือชื่อ อ.ที่ปรึกษาหลัก

6170331021 : MAJOR CHEMICAL ENGINEERING

KEYWORD: Polyaniline, PANI, Photovoltaic, Titanium dioxide, Electrodeposition
Akkharaphak Auisakul : Effects of Polyaniline Thickness on Photovoltaic Properties of PANI/TiO₂ Photovoltaic Cells. Advisor: Asst. Prof. Palang Bumroongsakulsawat, Ph.D.

Polyaniline (PANI) is a cheap conducting polymer that exhibits p-type properties with high conductivity and unique redox properties. In this work, PANI was synthesized directly on TiO₂/FTO substrates by electropolymerisation from acidic aqueous solutions of aniline to form PANI/TiO₂ p-n junctions with photovoltaic properties. The thickness of the PANI layer was varied by varying electrodeposition time: 15, 30, and 45 min at the same current density of 2 mA cm⁻². The thicknesses of the deposited PANI layers were examined with Scanning Electron Microscope (SEM). Short-circuit currents (I_{sc}) and open-circuit voltages (V_{oc}) of fabricated Pt/PANI/TiO₂/FTO cells are investigated. It was found that the PANI electrodeposition time at least 30 min corresponding to a PANI thickness of 399 nm was required for the cell to exhibit significant photovoltaic properties. Furthermore, the TiO₂ nanorods that is a remarkable morphology of the n-type TiO₂ was synthesized by electrochemical anodization of titanium in a fluoride-based electrolyte with varying anodization times: 45 and 60 min at the constant potential of 60 V. It was found that the anodization time at 60 min is the sufficient condition for the PANI electrodeposition at 45 min to exhibit photovoltaic properties.

Field of Study: Chemical Engineering

Student's Signature

Academic Year: 2019

Advisor's Signature

ACKNOWLEDGEMENTS

I would first like to thank you my clever advisor, Assistant Professor Palang Bumroongsakulsawat of the Faculty of Engineering at Chulalongkorn University, who is a kind and gentle person. I was obtained a lot of knowledge, electrochemical techniques, the system of a thinking process, and a good attitude from him. I appreciate working with my advisor because I always improve myself while doing the thesis. My advisor consistently allowed this paper to be my own work, but steered me in the right the direction whenever he thought I needed it.

I would like to thank the experts who were involved in the validation survey for this research project: Professor Sarawut Rimdusit of the Faculty of Engineering at Chulalongkorn University for his kind supervision over this thesis as the chairman, Assistant Professor Paravee Vas-Umnuay of the Faculty of Engineering at Chulalongkorn University for many pieces of advice in this thesis, and Assistant Professor Pornchai Bumroongsri of the Faculty of Engineering at Mahidol University for giving me time to a committee for my thesis.

Finally, I would like to thank you for the suggestions and useful help from the seniors and friends in the Center of Excellence on Catalysis and Catalytic Reaction Engineering, who always provide encouragement and assistance along with the study.

Akkharaphak Auisakul

TABLE OF CONTENTS

	Page
.....	iii
ABSTRACT (THAI)	iii
.....	iv
ABSTRACT (ENGLISH)	iv
ACKNOWLEDGEMENTS	v
TABLE OF CONTENTS	vi
LIST OF TABLES	ix
LIST OF FIGURES.....	x
CHAPTER 1 INTRODUCTION	1
1.1 Background	1
1.2 Objectives.....	3
1.3 Working scope.....	3
1.4 Expected benefits.....	4
1.5 Research plan.....	4
CHAPTER 2 THEORY.....	5
2.1 Photovoltaic cells.....	5
2.1.1 Photovoltaic parameters	6
2.1.2 Organic photovoltaic cells.....	9
2.2 Conducting polymers	10
2.3 Band theory	11
2.4 Semiconductor.....	12

2.5 Polyaniline.....	12
2.5.1 Structure of polyaniline	13
2.5.2 Synthesis of polyaniline	14
2.5.3 Polymerisation mechanism of aniline	15
2.5.4 Properties of polyaniline.....	19
2.6 Titanium dioxide.....	21
2.6.1 TiO ₂ nanorods.....	21
CHAPTER 3 LITERATURE REVIEWS	25
3.1 Comparison of photovoltaic properties between PANI and PEDOT:PSS.....	25
3.2 Electrochemical polymerisation of polyaniline on substrate	28
3.3 Morphology of Polyaniline.....	31
3.4 Polyaniline in photovoltaic cells.....	37
3.5 Synthesis of TiO ₂ nanorods.....	40
CHAPTER 4 MATERIALS AND METHODS.....	44
4.1 Materials	44
4.2 Synthesis of TiO ₂ nanorods.....	44
4.3 Electrodeposition of PANI on substrates.....	45
4.4 Characterization and the electrochemical performances.....	46
CHAPTER 5 RESULTS AND DISCUSSION	48
5.1 Morphology.....	48
5.2 FTIR spectra	55
5.3 Cyclic voltammogram	56
5.4 EIS spectra.....	60
CHAPTER 6 CONCLUSION AND RECOMMENDATIONS	66

6.1 Conclusion66

6.2 Recommendations66

REFERENCES.....68

VITA72



LIST OF TABLES

	Page
Table 1.1 Research plan.....	4
Table 5.2 I_{SC} and V_{OC} parameters of the PANI/porous TiO_2 PV cells that was deposited PANI15, PANI30, and PANI45 under 100 mW/cm^2	57
Table 5.3 I_{SC} and V_{OC} parameters of the PANI/ TiO_2 nanorods PV cells with the different TiO_2 nanorods anodization times that was deposited PANI30 and PANI45 under 100 mW/cm^2	59
Table 5.4 Sheet resistance (R_s) and charge transfer resistance (R_{ct}) of the PANI/porous TiO_2 PV cells that was deposited PANI15, PANI30, and PANI45.	62
Table 5.5 Sheet resistance (R_s) and charge transfer resistance (R_{ct}) of the PANI/ TiO_2 nanorods PV cells with the different TiO_2 nanorods anodization times that was deposited PANI30 and PANI45.....	64

LIST OF FIGURES

	Page
Figure 2.1 Cross-sectional view of fabricated PV cell [1].	5
Figure 2.2 The J-V characteristics of a p-n junction in the dark and under illumination [11].	6
Figure 2.3 a) The I-V characteristics curve of a p-junction in the dark and b) under illumination [12].	7
Figure 2.4 The I-V curve of the PV cell, when generating energy effect to the I-V curve is inverted to the current axis [12].	8
Figure 2.5 Chemical structure of the most common CPs [13].	10
Figure 2.6 Energy band diagram of metal, semiconductor, and insulator.	12
Figure 2.7 The redox reaction of PANI in different oxidation states [16].	13
Figure 2.8 Chemical structure of PANI in different oxidation states [8].	14
Figure 2.9 Oxidation of aniline during electrochemical polymerisation [7].	15
Figure 2.10 Radical coupling and re-aromatisation of aniline during electrochemical polymerisation [7].	16
Figure 2.11 Chain propagation of aniline during electrochemical polymerisation [7]. .	16
Figure 2.12 Oxidation and doping of the PANI during electrochemical polymerisation [7].	17
Figure 2.13 Overview of electrochemical polymerisation of aniline on substrate [16].	18
Figure 2.14 Cyclic voltammogram of PANI film on a Pt electrode in 1 M HCl at a scan rate 0.1 V s^{-1} . (The potentials at which structure and colour changes occur and the change in the potential of the second redox reaction with pH are shown as well) [7].	19

Figure 2.15 The doping of EB with protons to form the conducting emeraldine salt (PANI/HA) form of PANI (a polaron lattice) [7].	20
Figure 2.16 (a) The vectorial electron transport along the nanotubes axis and (b) the electrochemical cell of TiO ₂ nanorods synthesis [17].	22
Figure 2.17 The three stages of TiO ₂ nanorods potentiostatic anodization and the corresponding current density - time (j-t) diagram [17].	23
Figure 3.1 (a) Optical transmittance spectra of PEDOT:PSS and PANI films and (b) Photoelectron emission spectra of PEDOT:PSS and PANI films [5].	25
Figure 3.2 The PV characteristics of PEDOT:PSS/n-GaN/sapphire (0 0 0 1) and PANI/n-GaN/sapphire (0 0 0 1) samples under AM1.5 light irradiation [5].	25
Figure 3.3 Transmittances of PEDOT:PSS, PSSA-g-PANI and PSSA-g-PANI/GO composite films, where the film thickness is 40 nm [6].	26
Figure 3.4 The J-V curves measured under AM 1.5 G (100 mW/cm ²) of P3HT:P ₆₁ BM PV cell with PEDOT:PSS, PSSA-g-PANI, and PSSA-g-PANI/GO composites as HTL [6].	27
Figure 3.5 IR spectrum of PANI that synthesis by electropolymerisation method with constant potential at +0.5 V for 5 min [20].	29
Figure 3.6 (a) DSC thermogram and (b) Diffraction pattern of PANI that synthesis by electropolymerisation method with constant potential at +0.5 V for 5 min [20].	30
Figure 3.7 SEM images of PANI that synthesized by Budi, S. (2020)	31
Figure 3.8 The pulse current density diagram [21].	31
Figure 3.9 SEM images of PANI with the different pulsed current densities: (a) 10 mA cm ⁻² , (b) 30 mA cm ⁻² , (c) 75 mA cm ⁻² , (d) 125 mA cm ⁻² , and (e) 200 mA cm ⁻² [21].	32
Figure 3.10 SEM images of PANI with the different relaxation times (t _{off}): (a) 0 s, (b) 0.25 s, (c) 0.5 s, (d) 1.0 s, and (e) 2.0 s [21].	33
Figure 3.11 SEM images of PANI with the different pulse times (t _{on}): (a) 0.1 s, (b) 0.25 s, (c) 0.5 s, (d) 1.0 s, and (e) 2.0 s [21].	34

<i>Figure 3.12 SEM images of PANI with the different temperatures (a) 15 °C, (b) 25 °C, (c) 35 °C, (d) 45 °C, and (e) 55 °C [21].</i>	35
<i>Figure 3.13 SEM images of PANI with the different aniline concentrations: (a) 0.05 M, (b) 0.1 M, and (c) 1.0 M [21].</i>	36
<i>Figure 3.14 SEM images of PANI with the different perchloric acid concentrations: (a) 0.05 M, (b) 0.1 M, (c) 1.0 M, and (d) 2.0 M [21].</i>	37
<i>Figure 3.15 (a) Light absorption and (b) CV characterization of PANI films with the different doping ratios [15].</i>	38
<i>Figure 3.16 The J-V curves of device with the different PANI films as anode buffer layers devices tested in the dark and under 100 mW cm⁻² illumination [15].</i>	38
<i>Figure 3.17 The images of PANi-PSI films deposited on TiO₂/FTO/glass substrates. Samples were prepared from potentiostatic polymerisation at +6.5 V, for A) 90, B) 120, and C) 240 s and the PV efficiency diagram of Ag/PAni-PSI/TiO₂ PV cells prepared with active layer thicknesses polymerized for 90, 120, or 240 s [19].</i>	39
<i>Figure 3.18 The I-V curves for Ag/PAni-PSI/TiO₂ and Ag/PAni-only/TiO₂ solid-state PV cells tested in the dark and under AM 1.5 solar simulated illumination [19].</i>	40
<i>Figure 3.19 FE-SEM images of TiO₂ nanorods that anodized at 20 V for 60 min with 1.5% NH₄F and glycerin : D.I. water (70 : 30) electrolyte: (a) top view, (b) cross-sectional view, and (c) bottom view and with (d) glycerin : D.I. water (70 : 30) without NH₄F electrolyte on top-view [22].</i>	41
<i>Figure 3.19 XPS spectra of TiO₂ nanorods that anodized at 20 V for 60 min in the different electrolytes: glycerin : D.I. water (70 : 30) with 1.5% NH₄F and without NH₄F electrolyte [22].</i>	41
<i>Figure 3.20 FE-SEM images of TiO₂ nanorods that anodized at 50 V in 0.5 wt% NH₄F and ethylene glycol electrolyte: (a) top view, (b) cross-sectional view, (c) bottom view, and (d) digital image of Ti sputtered FTO glass and the transparent TiO₂ nanorods after Ti anodization [23].</i>	42

Figure 4.1 The synthesis of the TiO_2 nanorods by electrochemical anodization of titanium in a fluoride-based electrolyte cell.	45
Figure 4.2 The glassware, RE, CE, and WE for electrochemical polymerisation	46
Figure 4.3 The cross - sectional view of the fabricated PANI/ TiO_2 PV cells.	47
Figure 5.1 Cross-sectional SEM image of the TiO_2 /FTO layers.	48
Figure 5.2 Cross-sectional SEM images of PANI15/ TiO_2 /FTO layers.	49
Figure 5.3 Cross-sectional SEM images of PANI30/ TiO_2 /FTO layers.	49
Figure 5.4 Cross-sectional SEM images of PANI45/ TiO_2 /FTO layers.	49
Figure 5.5 Calibration curve of the PANI average thicknesses with the different PANI electrodeposition times: 15, 30 and 45 min.	50
Figure 5.6 Cross-sectional SEM-EDX maps of the PANI45/ TiO_2 /FTO layers: (a) cross-sectional SEM image of PANI45/ TiO_2 /FTO and the elemental maps of (b) carbon, (c) nitrogen, (d) silicon, (e) tin, and (f) titanium.	50
Figure 5.7 SEM images of PANI30 on the TiO_2 /FTO substrate with the different	51
Figure 5.8 SEM images of the TiO_2 nanorods that anodized at 60 V in 0.9 wt% NH_4F , 1.0 wt% H_2O , and ethylene glycol electrolyte with the different anodization times: 45 and (b) 60 min.	52
Figure 5.9 Digital images of (a) the anodized TiO_2 nanorods with 0.8 wt% NH_4F , (b) the anodized TiO_2 nanorods at 45 V, (c) the anodized TiO_2 nanorods at 75 min, (d) the anodized TiO_2 nanorods at 45 and 60 min.	54
Figure 5.10 SEM images of TiO_2 nanorods45 that was deposited (a) PANI30 and (b) PANI45 and TiO_2 nanorods60 that was deposited (c) PANI30 and (d) PANI45.	54
Figure 5.11 FTIR spectra of PANI15, PANI30, and PANI45 on TiO_2 /FTO substrate glass.	55
Figure 5.12 The overlay cyclic voltammogram of the PANI/porous TiO_2 PV cells that was deposited PANI15, PANI30, and PANI45 in the dark and under 100 mW/cm^2	56

Figure 5.13 The overlay cyclic voltammogram of the PANI/TiO ₂ nanorods45 PV cells that was deposited with PANI30 and PANI45 in the dark and under 100 mW/cm ²	58
Figure 5.14 The overlay cyclic voltammogram of the PANI/TiO ₂ nanorods60 PV cells that was deposited with PANI 30 and PANI45 in the dark and under 100 mW/cm ² ...	59
Figure 5.15 The overlay Nyquist plots of the PANI/porous TiO ₂ PV cells that was deposited PANI15, PANI30, and PANI45.	61
Figure 5.16 The equivalent circuit proposed to fit the Nyquist plots of the PANI/porous TiO ₂ PV cells that was deposited PANI15, PANI30, and PANI45.	62
Figure 5.17 The overlay Nyquist plots of the PANI/TiO ₂ nanorods45 PV cells that was deposited PANI30 and PANI45.....	63
Figure 5.18 The overlay Nyquist plots of the PANI/TiO ₂ nanorods60 PV cells that was deposited PANI30 and PANI45.....	63
Figure 5.19 The equivalent circuit proposed to fit the Nyquist plots of the PANI/TiO ₂ nanorods45 PV cells that was deposited PANI 30 and PANI45.....	64
Figure 5.20 The equivalent circuit proposed to fit the Nyquist plots of the PANI/TiO ₂ nanorods60 PV cells that was deposited PANI30 and PANI45.....	65

CHAPTER 1

INTRODUCTION

1.1 Background

Nowadays, the demand for energy is increasing due to the increase in various industries. In which the energy production process can be produced from many energy resources such as coal, petroleum, and natural gas that is non-renewable energy sources [1]. Additionally, the energy production process of non-renewable energy sources will release carbon dioxide (CO₂) gas, which is also known as one of the greenhouse gases that can destroy ozone (O₃) in the atmosphere affect long-term global warming in the average temperature of the earth's climate system. Therefore, we can reduce CO₂ gas by reducing the use of energy from non-renewable energy sources, which is the mainstream energy and turning our attention to energy from renewable energy sources such as wind energy, hydroelectric power, biomass energy, geothermal energy and solar energy [1]. Solar energy is the most interesting because of remarkable characteristics such as the most plentiful, illimitable, clean of all the renewable energy resources, and energy from solar cells base on the photovoltaic phenomenon that does not combustion, it does not cause certain substances that are harmful to the environment.

The photovoltaic (PV) cells are still interesting to study as there are many types of solar cells such as hybrid material solar cells, dye-sensitized solar cells, and organic photovoltaic. Organic photovoltaic (OPV) cells are the most interested and considered as an alternative to the standard silicon-based PV cells due to it is composed of carbon-rich conducting polymers and can be tailored to enhance a specific function of the cells, such as sensitivity to a certain type of light [2]. The main causes of interest to the development of OPV cells technology are low cost, thinner, more flexible, high transparency, and cooperative with a wide range of lighting conditions [1]. Although, crystalline silicon solar cell has more efficient and longer operating lifetimes than OPV cells, but OPV cells could be low cost to

manufacture in high volumes. Moreover, OPV cells can be applied to a variety of PV materials that modified OPV cells to improve PV applications [2].

Titanium dioxide (TiO_2) is a metal oxides semiconductor, which is a distinctive n-type material. It has high optical and thermal stability, low toxicity, environmental green, less expensive, corrosion resistance, and ease of synthesis [1]. It was a suitable material for applied OPV cells. TiO_2 nanorods are another morphology of TiO_2 that have a remarkable advantage such as a direct pathway for electron transfer with fewer grain boundaries due to the existence of a continuous wall, the vectorial electron transport without significant losses, and high light absorption due to the light trapping effect [3].

Polyaniline (PANI) is a homopolymer, that exhibits p-type properties with high conductivity, good electrocatalytic activity and unique redox properties associated with the chain nitrogen, it's an attractive polymer to modified OPV cells [4].

In previous research, Matsuki, N. (2011) and Bae, S. (2014) has a comparison of p-type materials between PANI and poly(3,4-ethylenedioxythiophene):poly(styrene sulfonate) (PEDOT:PSS) with PV properties. It was found that PV cells with PANI exhibit higher optical transmittance than PEDOT:PSS, in which both films had a similar thickness [5, 6]. Furthermore, PV cells with PANI has higher electrical conductivity and higher hole transport performance as compared to PV cells with PEDOT:PSS [6].

According to our previous work, PANI can be processed from acidic aqueous solutions of aniline into a thin film of PANI by electropolymerisation method. Moreover, the molecular structure of PANI has three oxidation states including leucoemeraldine, emeraldine, and pernigraniline that may contain either benzenoid or quinonoid or both of them at the different proportions. The oxidation state of PANI that alternate to be a semiconductor is emeraldine base (blue), it is known as the most useful form of due to its high stability at room temperature and it is composed of benzenoid units and one quinonoid unit that can adjust number of units by varying electropolymerisation synthesis procedure [7, 8].

In this work, PANI was synthesized directly on TiO_2/FTO substrates glass by electropolymerisation from acidic aqueous solutions of aniline to form p-n junctions

with PV properties. The thickness of the PANI layer was varied by varying electrodeposition times: 15, 30, and 45 min at the same constant current density of 2 mA cm^{-2} . Therefore, the optimization of PANI thickness directly affects PV properties. OPV cells with cheap PANI materials were assembling in Pt/PANI/TiO₂/FTO architecture. Furthermore, TiO₂ nanorods that is a remarkable morphology of TiO₂ was synthesized by electrochemical anodization of titanium in a fluoride-based electrolyte with varying anodization times: 45 and 60 min at the constant potential of 60 V. TiO₂ nanorods and TiO₂/FTO substrates glass were serve as a n-type material for electrodeposition of a p-type PANI to fabricate the PANI/TiO₂ PV cells.

1.2 Objectives

- 1) To fabricate of the PANI/TiO₂ PV cells in Pt/PANI/TiO₂/FTO architecture.
- 2) To synthesize and characterize the PANI films by electropolymerisation from HCl acid aqueous solutions of aniline on titanium dioxide (TiO₂) - coated fluorine-doped tin oxide (FTO) substrates as PV cells.
- 3) To study and optimize the thicknesses of the PANI films in difference electrodeposition times that improve PV cells efficiency.
- 4) To synthesize the TiO₂ nanorods using as a n-type substrate for the PANI/TiO₂ PV cells by electrochemical anodization method from a fluoride-based electrolyte.

จุฬาลงกรณ์มหาวิทยาลัย
CHULALONGKORN UNIVERSITY

1.3 Working scope

- 1) Synthesize the different thicknesses of the PANI on the TiO₂/FTO substrate by varying electrodeposition times: 15, 30, and 45 min at the same current density of 2 mA cm^{-2} with chrono potentiometry ($\Delta t > 1 \text{ ms}$) technique.
- 2) Short-circuit currents (I_{sc}) and open-circuit voltages (V_{oc}) parameters of the PANI/TiO₂ PV cells in the different thicknesses of PANI were measured by cyclic voltammetry potentiostatic technique with constant potential at -0.01 V and scan rate 0.05 V s^{-1} .
- 3) R_s and R_{ct} parameters of the PANI/TiO₂ PV cells in the different thicknesses of PANI were measured by FRA impedance potentiostatic technique with

constant potential at 0 V, the perturbation amplitude 10^{-2} , and frequency range were between 10^6 and 10^{-1} Hz.

- 4) Synthesis of the TiO_2 nanorods by varying anodization times: 45 and 60 min at the constant potential of 60 V.

1.4 Expected benefits

This work will fabricate the PANI/ TiO_2 PV cells in Pt/PANI/ TiO_2 /FTO architecture by ease method and will optimize the thickness of the p-type PANI that appropriate to form a p-n junction with the n-type TiO_2 by varying electrodeposition times for improving PV properties. Moreover, the TiO_2 nanorods were applied in OPV cell to study as a remarkable n-type material.

1.5 Research plan

Table 1.1 Research plan

Activities	Period														
	2019						2020								
	Jul	Aug	Sep	Oct	Nov	Dec	Jan	Feb	Mar	Apr	May	Jun			
1. Literature survey	←			→											
2. Experimental design			←						→						
3. PANI electrodeposition and fabrication of PV cells			←						→						
4. Characterization of PV cells								←					→		
5. Research discussion and write thesis									←					→	

CHAPTER 2

THEORY

2.1 Photovoltaic cells

The photovoltaic (PV) cells or solar cells are a potent electrical device that is made up of semiconductor materials, which converts the solar radiant energy ultimately into electrical energy without acoustic or chemical pollution during operation by absorbs solar radiation (photons) [9]. The three main components of PV cells consist of n-type material, p-type material, and counter electrode. N-type material is an extrinsic semiconductor that has a large number of electrons, which are caused by doping of atoms with five valence electrons. On the other hand, p-type material is an extrinsic semiconductor with many holes, which are caused by the addition of atoms with three valence electrons. The p-n junction is caused by the combination of p-type material and n-type material, resulting in a combination of electron of n-type material and hole of p-type material. The atom at the junction of the n-type material lost the electron to create a positive electric charge which resist the movement of the hole from p-type material, while the atom at the junction of the p-type material has an excess electron resulting in a negative electric charge, which will resist the free electron that may cross from n-type material to p-type material. A counter electrode plays the most important role in collecting electrons from the external circuit to complete the current cycle. In general, a platinum (Pt) is commonly used as a counter electrode.

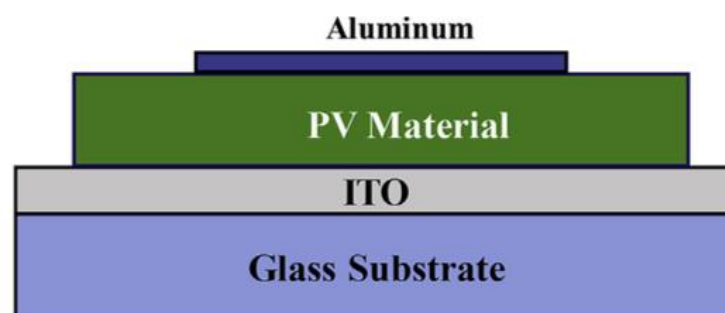


Figure 2.1 Cross-sectional view of fabricated PV cell [1].

The PV cells have been developed for decades, with three generations divided according to technologies consisting of technologies based on Si wafer, thin film technologies, until new emerging technologies are the newest generation such as quantum dot, hybrid materials PV cells, dye sensitized PV cells, and organic PV cells.

2.1.1 Photovoltaic parameters

The PV performance is depending on the photoelectric effect of semiconductor [10]. The PV performance of photovoltaic cells can characterize by various parameters such as the peak power (P_{max}), the short-circuit current density (J_{sc}), the open circuit voltage (V_{oc}), the fill factor (FF), and the conversion efficiency (η) [11]. These parameters are detected and calculated from **Figure 2.2** [11].

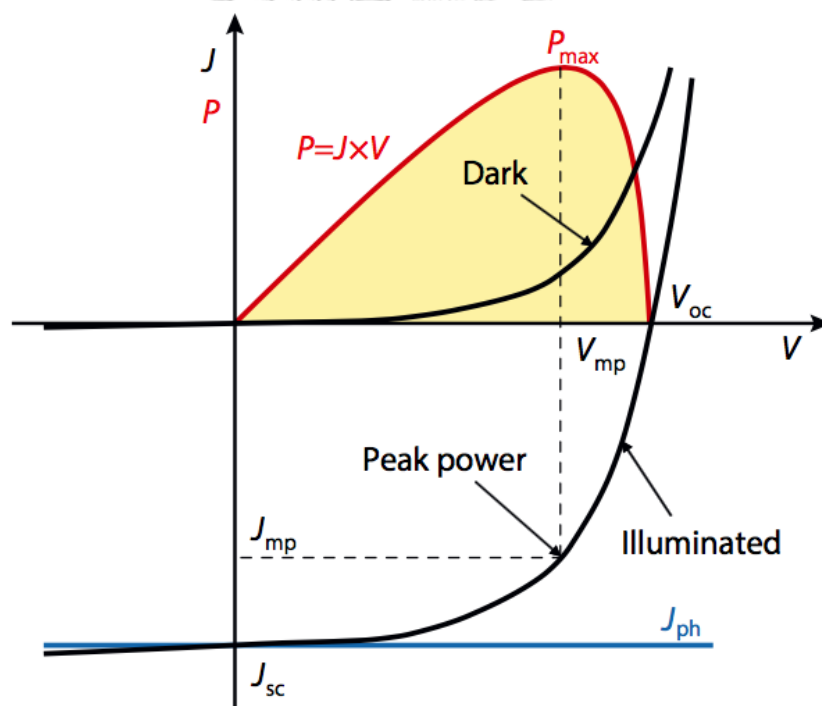


Figure 2.2 The J - V characteristics of a p - n junction in the dark and under illumination [11].

The measurement of the J - V characteristics should be performed under standard test conditions (STC), which is total irradiance on the PV cell measured is 1000 W m^{-2} for a reliable result [11]. The air mass (AM) coefficient can determined from equation:

$AM=1/\cos(z)$, where z is the zenith angle, is an assume point directly above a particular location, in degrees. The industrial standard is the AM1.5 spectrum that corresponds to the zenith of 48.2° and the temperature of the PV cell should be constant at 25°C [11].

1) Current voltage curve

The current-voltage (I-V) characteristics of a p-junction in the dark was show in **Figure 2.3 a)** and then when the light was absorbed on PV cell, the I-V curve shift down to the fourth quadrant to generate solar energy that show in **Figure 2.3 b)** [12].

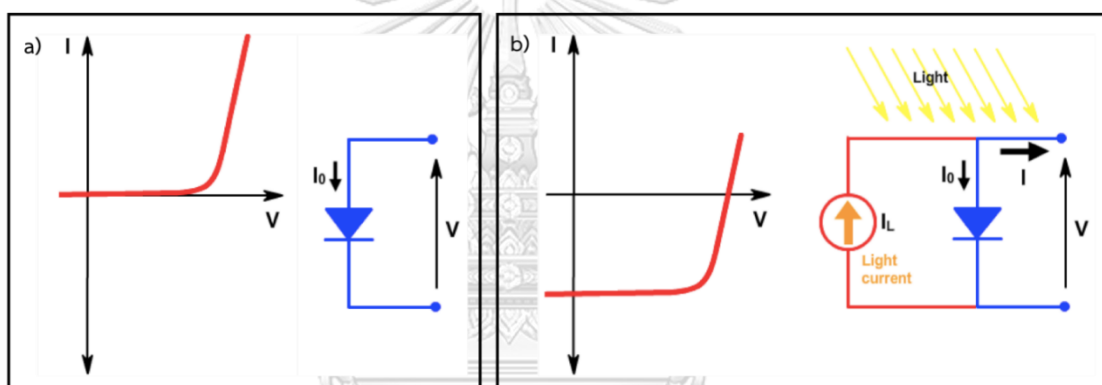


Figure 2.3 a) The I-V characteristics curve of a p-junction in the dark and **b)** under illumination [12].

The output current (I) can calculate from below equation, where I_L is light generate current, I_0 is dark saturation current, q is electron charge, V is the voltage, n is the ideality factor of diode, k is boltzmann constant, and T is the temperature [12].

$$I = I_L - I_0 \left[\exp \frac{qV}{nkT} \right]$$

As show in **Figure 2.4**, when the PV cell is generating energy effect to the I-V curve is inverted to the current axis [12]. Moreover, the maximum power parameters were

from **Figure 2.4**, which including the maximum power output (P_{MP}), the maximum voltage (V_{MP}), and the maximum current (I_{MP}) [12].

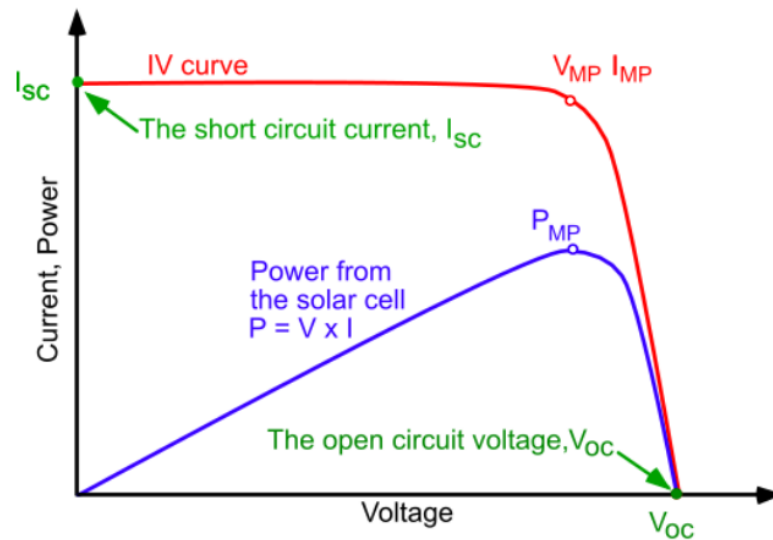


Figure 2.4 The I-V curve of the PV cell, when generating energy effect to the I-V curve is inverted to the current axis [12].

2) Short-circuit current

The current is flowing through the external circuit when the electrodes of the PV cell are short-circuited called the short-circuit current (I_{sc}), which depends on the photon flux incident on the PV cell that obtained from the spectrum of the incident light [11]. The short-circuit current density (J_{sc}) is the ratio of I_{sc} and the area of the PV cell. The J_{sc} is useful in terms of removing the dependence of the PV cell area onto I_{sc} due to I_{sc} depend on the PV cell area [10]. The crystalline silicon PV cell is measure under STC a maximum possible of J_{sc} is 46 mA cm^{-2} [11].

3) Open-circuit voltage

The open-circuit voltage (V_{oc}), is the voltage that the current not flow through the external circuit, is the maximum voltage that the PV cell can generate in no load condition [10]. The V_{oc} corresponding to the forward bias voltage [11].

$$V_{oc} = \frac{E_g}{q} - \frac{nkT}{q} \left[\ln \frac{I_{0 \max}}{I_{sc}} \right]$$

Where, E_g is the energy band gap and I_0 max is the maximum dark saturation current. The V_{oc} of crystalline silicon PV cell in laboratory is 720 mV under STC, while the commercial PV cells normally have V_{oc} 600 mV [11].

4) Fill factor

The fill factor (FF) is the proportion between the actual maximum power output (P_{MP}) that generated by the PV cell and the theoretical power output (P_T) [11].

$$FF = \frac{P_{MP}}{P_T} = \frac{V_{MP}I_{MP}}{V_{OC}I_{SC}}$$

Their parameters were obtaining from the I-V curve of the PV cell as show in **Figure 2.4** [12]. The FF is another parameter, which is typically used to identify PV performance of PV cell. The FF of crystalline silicon PV cell in laboratory is in the range of 0.75 - 0.80 under STC [11].

5) Conversion efficiency

The conversion efficiency (η) is the proportion between the actual maximum power output (P_{MP}) that generated by the PV cell and the power input (P_{IN}) that commonly perform and measured under the STC. The η of crystalline silicon PV cell in laboratory is in the range of 17 - 18% under STC [11].

$$\eta = \frac{P_{MP}}{P_{IN}} = \frac{V_{MP}I_{MP}}{I_{IN}A}$$

Where, I_{IN} is the intensity of incident light that equal to 1000 W m^{-2} under STC and A is the surface area of PV cell.

2.1.2 Organic photovoltaic cells

Organic photovoltaic (OPV) cells are composed of carbon-rich conducting polymers and can be tailored to enhance a specific function of the cell, such as

sensitivity to a certain type of light [2]. The main causes interest to the development of organic PV cell technology are less expensive, thinner, more flexible, amenable to a wide range of lighting conditions and low material consumption results in a high absorption coefficient [1]. Although, Crystalline silicon PV cell has more efficient and longer operating lifetimes than OPV cells, but OPV cells could be low cost to manufacture in high volumes. Moreover, OPV cells can be applied to a variety of PV materials that modified OPV to improve photovoltaic applications [2].

2.2 Conducting polymers

Conducting polymers (CPs) are an organic based polymer, which can act as a semiconductor or a conductor that conduct electricity due to delocalization of pi-electrons [4]. Additionally, CPs are the class of materials, which are fit for PV application and device fabrication. This is because of out-standing characteristics such as intrinsically stable photoexcitation with visible light, high photon harvesting efficiency, tunable band gap engineering on the entire visible spectral range and large charge generation when mixed with electron acceptor materials [1].

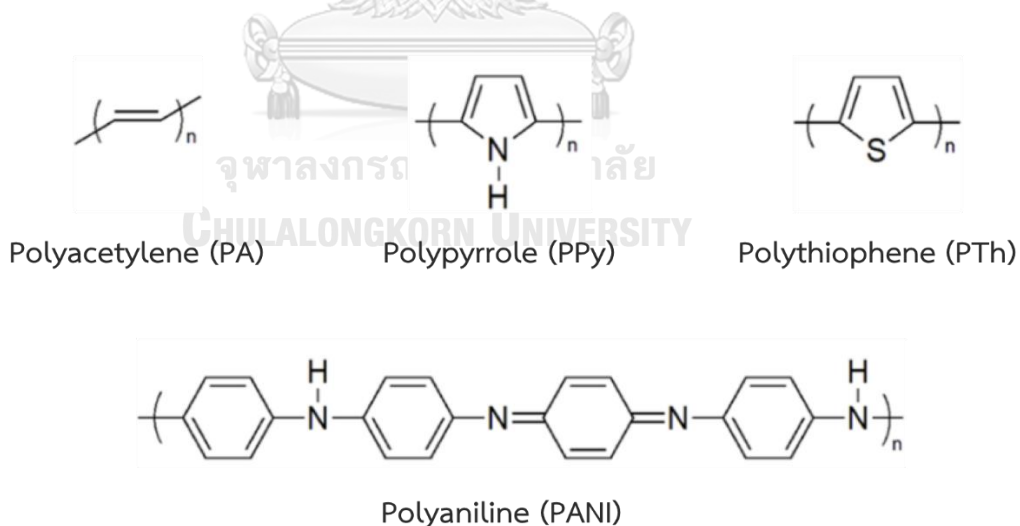


Figure 2.5 Chemical structure of the most common CPs [13].

Their chemical structures have a pi-conjugated molecule, that consists of a single bond alternating with a double bond. Electrical polymerisation also known as

"doping process" relies on oxidation-reduction reaction or Protonation depending on the type of polymer. CPs synthesized in the form of nanomaterials are of particular interest because their properties significantly change from the properties of their bulk counterpart [4]. As show in **Figure 2.5**, the most common examples are polyacetylene (PA), polypyrrole (PPy), polythiophene (PTh), and polyaniline (PANI). Ppy is widely used in tissue engineering and anti-corrosion application while PTh is applied as biosensor and electrochromic devices. PANI has potential application in various fields such as electrode materials for batteries, chemical sensor, gas sensor, microwave absorption, and PV cell [14].

2.3 Band theory

Band theory is a theory used to describe the electrical properties of solids, which are determined by the atomic energy level, the atomic composition, and the interaction between atoms in solid. The energy bands can be divided into three bands including valance band, energy gap band, and conduction band. The valance band is the lowest energy band that electron within this band is held in orbit atom. Therefore, the electron at the valance band has higher potential energy, while it has lower kinetic energy than the energy gap band that is the gap between the valance orbital and the external atoms. The electron at the conduction band is an electron with enough activation energy to release a bond electron from the valance band to become a free electron. Therefore, the electron at the conduction band has low potential energy, while it has high kinetic energy.

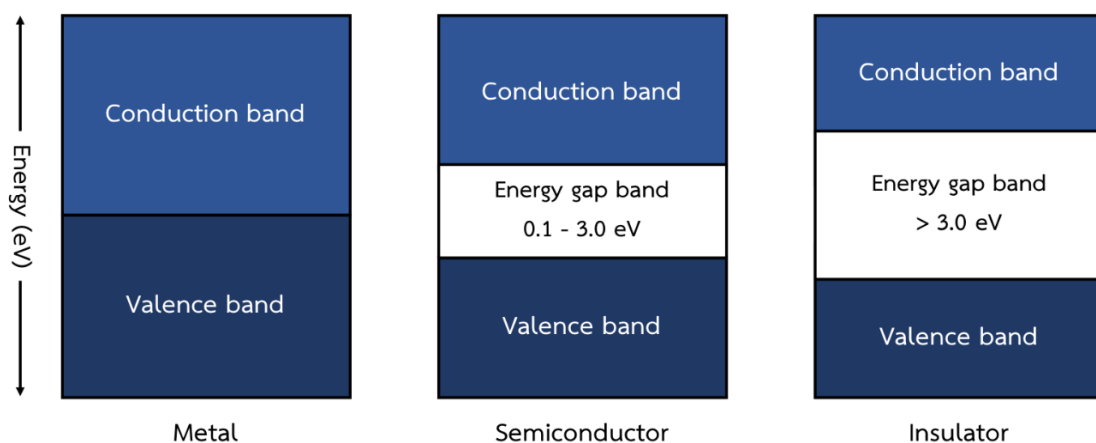


Figure 2.6 Energy band diagram of metal, semiconductor, and insulator.

2.4 Semiconductor

Semiconductor is a crystalline solid material that has electronic properties in the middle between metals and insulators, which can be used to create various electronic devices such as diodes, transistors, etc. The properties of semiconductor can explain by energy gap, in which valence electrons and conduction electrons, are allowed only in some energy values, with a forbidden band of energies between both [10]. The semiconductor allowing to become a conductor by either when electron not fully filled in valence band or when the band gap is very narrow, i.e. $E_g = 0.1 - 3.0$ eV, hence electrons can be excited by energy to separate from their atoms by jumping to a higher energy level into the conduction band by thermal or photochemical excitation methods [7]. The semiconductor can be divided into two types including intrinsic semiconductor and extrinsic semiconductor. An intrinsic semiconductor or undoped semiconductor has poor electrical conductivity compared to an extrinsic semiconductor because valence electrons are combined by following octet rule. Therefore, it is preferable to add other substances to create better electrical conductivity by doping, which has two types, n-type and p-type semiconductor.

2.5 Polyaniline

Polyaniline (PANI) is a homopolymer, it's an attractive polymer due to its relative high conductivity, good electrocatalytic activity, and unique redox properties associated with the chain nitrogen [4]. Extensive researches enable its various applications such as gas sensors, lithium batteries, light emitting diodes, and PV cell [15]. One of the potential applications of PANI is in solar cell where PANI has been used as counter electrode (CE) material in solar cell device [4]. Additionally, PANI has well electron conducting behaviors and redox behavior, high environmental stability, high controllable electrical, and high optical properties [1]. All these remarkable properties of PANI corresponding to the delocalized pi-electron structure. The PANI can be trap large amount of light due to high optical absorption coefficient [1].

2.5.1 Structure of polyaniline

Molecular structure of polyaniline has three oxidation state including leucoemeraldine (C_6H_4NH)_n (light yellow), emeraldine ($[C_6H_4NH]_2[C_6H_4N]_2$)_n (green - blue), and pernigraniline (C_6H_4N)_n (blue - violet) that show in **Figure 2.7** [16]. The PANI structure may contain either benzenoid or quinonoid, or both of them at different proportions.

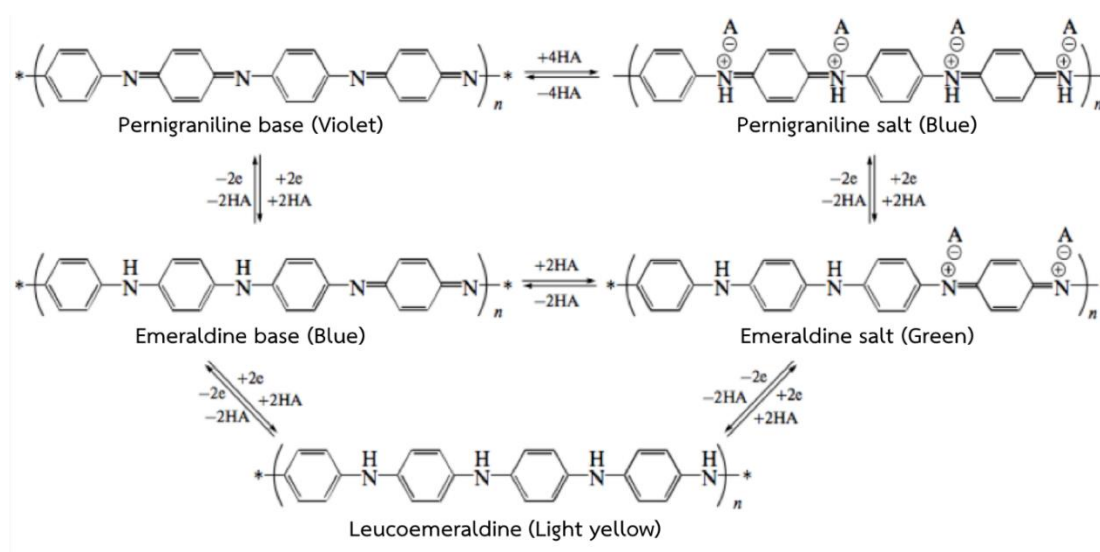


Figure 2.7 The redox reaction of PANI in different oxidation states [16].

The fully reduced leucoemeraldine state consists of benzenoid units where hydrogen atoms are attached to nitrogen atoms, on the other hand fully oxidized pernigraniline state consists of quinonoid units where no hydrogen atom are attached to nitrogen atoms [8]. Partially oxidized and partially reduced emeraldine state consists both of benzenoid and quinonoid units. The redox state of PANI is dependent on the ratio of m and n which represent benzenoid and quinonoid units, respectively, in PANI chains that show in **Figure 2.8** [8]. The proportion between benzenoid and quinonoid unit can be detected by the ratio of the intensities in Fourier transformation infrared (FTIR) spectrum in accordance with to benzenoid units near 1460 cm^{-1} and quinonoid units near 1560 cm^{-1} [8]. The state that alternate to be a semiconductor is emeraldine base (blue), it is known as the most useful form of PANI

due to its high stability at room temperature, it is composed of two benzenoid units and one quinonoid unit [7].

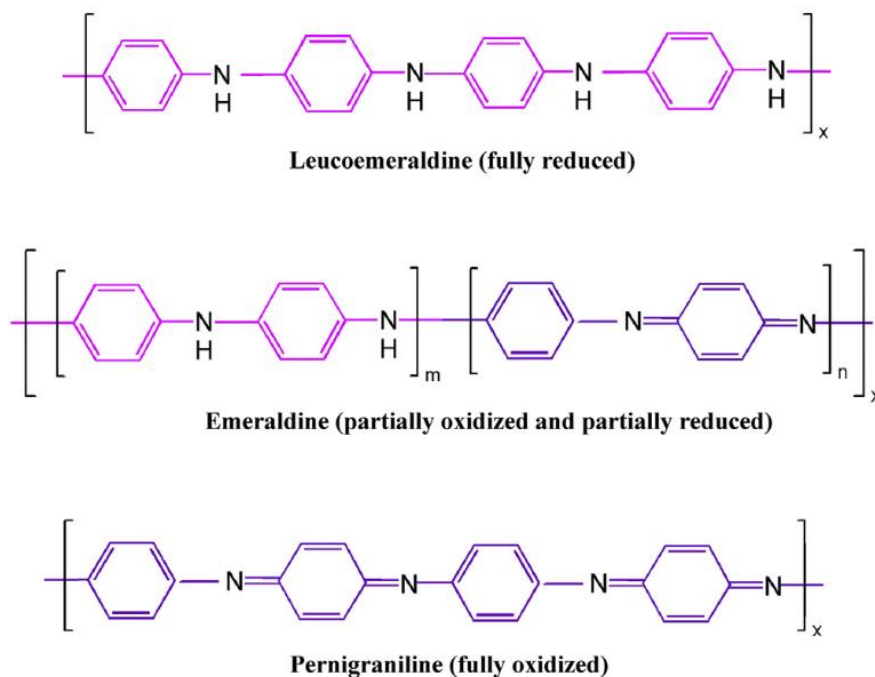


Figure 2.8 Chemical structure of PANI in different oxidation states [8].

2.5.2 Synthesis of polyaniline

PANI can be synthesized by several methods such as electrochemical oxidation of the monomers, chemical synthesis, enzyme-catalyzed polymerisation, and photochemically-initiated polymerisation [7]. The electrochemical polymerisation method, aniline is a monomer that is used as an initial molecule to form an oligomer and then the oligomer was oxidized by the applied potential to form a polymer that will electrodeposit on the substrate. Furthermore, electrochemical polymerisation methods involve three techniques to synthesize PANI including a constant voltage (potentiostatic), a variable current and voltage (potentiodynamic), and a constant current (galvanostatic) from an aqueous solution of aniline that is used as an electrolyte in this method [7]. The three-electrode system employed for electropolymerisation consists of a counter electrode e.g. platinum or titanium, a reference electrode e.g. Ag/AgCl, and a working electrode that can be a platinum

gold, glassy carbon or indium tin oxide (ITO) or fluoride tin oxide (FTO), which can be deposited PANI [7]. The advantage of electrochemical synthesis that distinguish from other synthesis method such as its simplicity, cost-effectiveness, and the performance of the process in a single section glass cell [4].

2.5.3 Polymerisation mechanism of aniline

The electrochemical polymerisation mechanism of aniline proceeds via a radical propagation mechanism as shown in **Figure 2.9 - 2.12** [7].

Step 1: Oxidation of monomer

Oxidation of monomer is an initial step that show in **Figure 2.9**, aniline is oxidized into radical cation by an aqueous acid solution, which subsist in three resonance forms. This step is the slowest step in the reaction, which is rate determining step in polymerisation reaction [7].

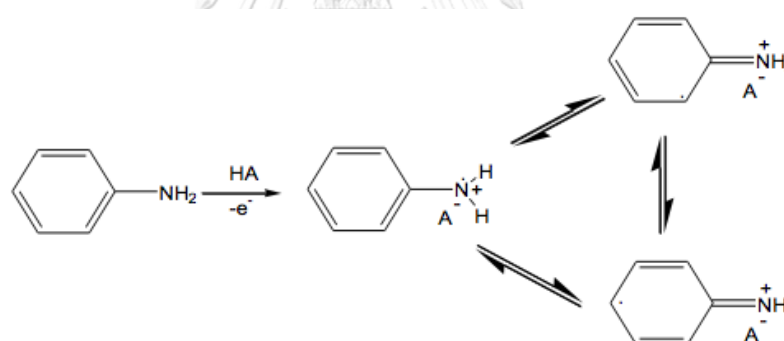


Figure 2.9 Oxidation of aniline during electrochemical polymerisation [7].

Step 2: Radical coupling and re-aromatisation

Radical coupling and re-aromatisation is an initial step, which occurs simultaneously with oxidation of aniline that show in **Figure 2.10**, in this step aniline radical cation will head to tail coupling with the *N*- and *para*- of other aniline radical cations to form dimer that can re-aromatisation into intermediate, *p*-aminodiphenylamine (PADPA), and then elimination of protons to obtain neutral state [7].

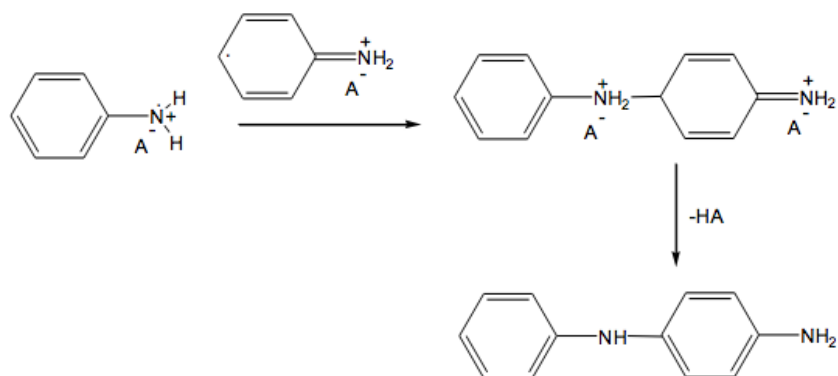


Figure 2.10 Radical coupling and re-aromatization of aniline during electrochemical polymerisation [7].

Step 3: Chain propagation for electrochemical synthesis

In chain propagation step for electrochemical synthesis that show in **Figure 2.11**, the dimer will oxidize on the surface of a working electrode to become a dimer radical cation at para position of nitrogen atom that will couple with an aniline cation to increase unit of polymer [7].

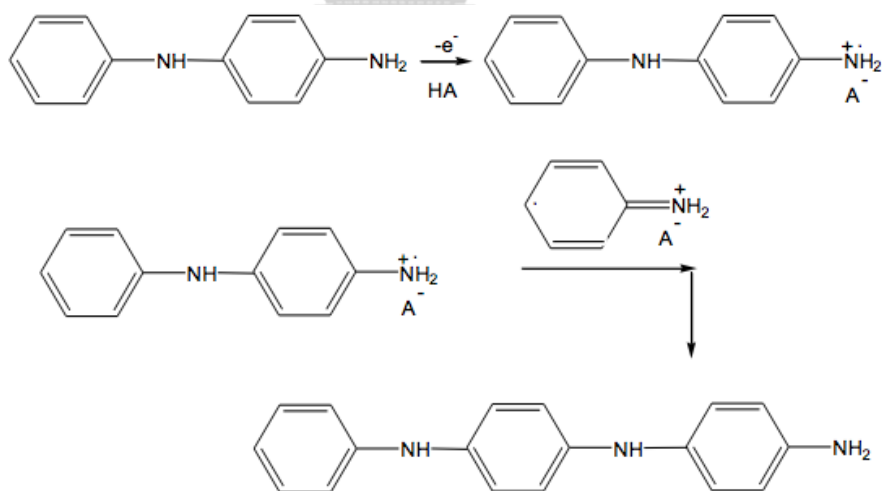


Figure 2.11 Chain propagation of aniline during electrochemical polymerisation [7].

Step 4: Oxidation and doping of the polymer for electrochemical synthesis

Oxidation and doping of the polymer for electrochemical synthesis, which show in **Figure 2.12**, are the oxidation step of PANI into PANI radical cation that can extend the chain of polymer by doping in aqueous acid solution [7].

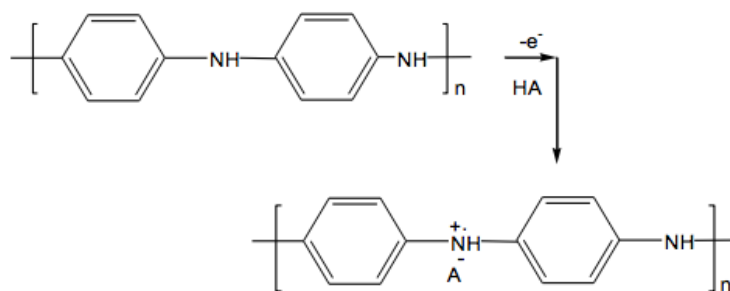


Figure 2.12 Oxidation and doping of the PANI during electrochemical polymerisation [7].

The electrochemical polymerisation of aniline on substrate was shown in **Figure 2.13** [12]. First of all, the hard template or substrate was applied current or potential to become partially negative charge substrate that can adsorb anilinium cation or aniline radical cation from an electrolyte solution and then anilinium cation on their surface was oxidized into reactive species (oxidized anilinium cation) [16]. Finally, the oxidized anilinium cation adsorbed on surface substrate was polymerised to obtain PANI thin films on substrate, which has different oxidation states and morphologies that depend on component of an electrolyte solution and electrochemical polymerisation technique [16].

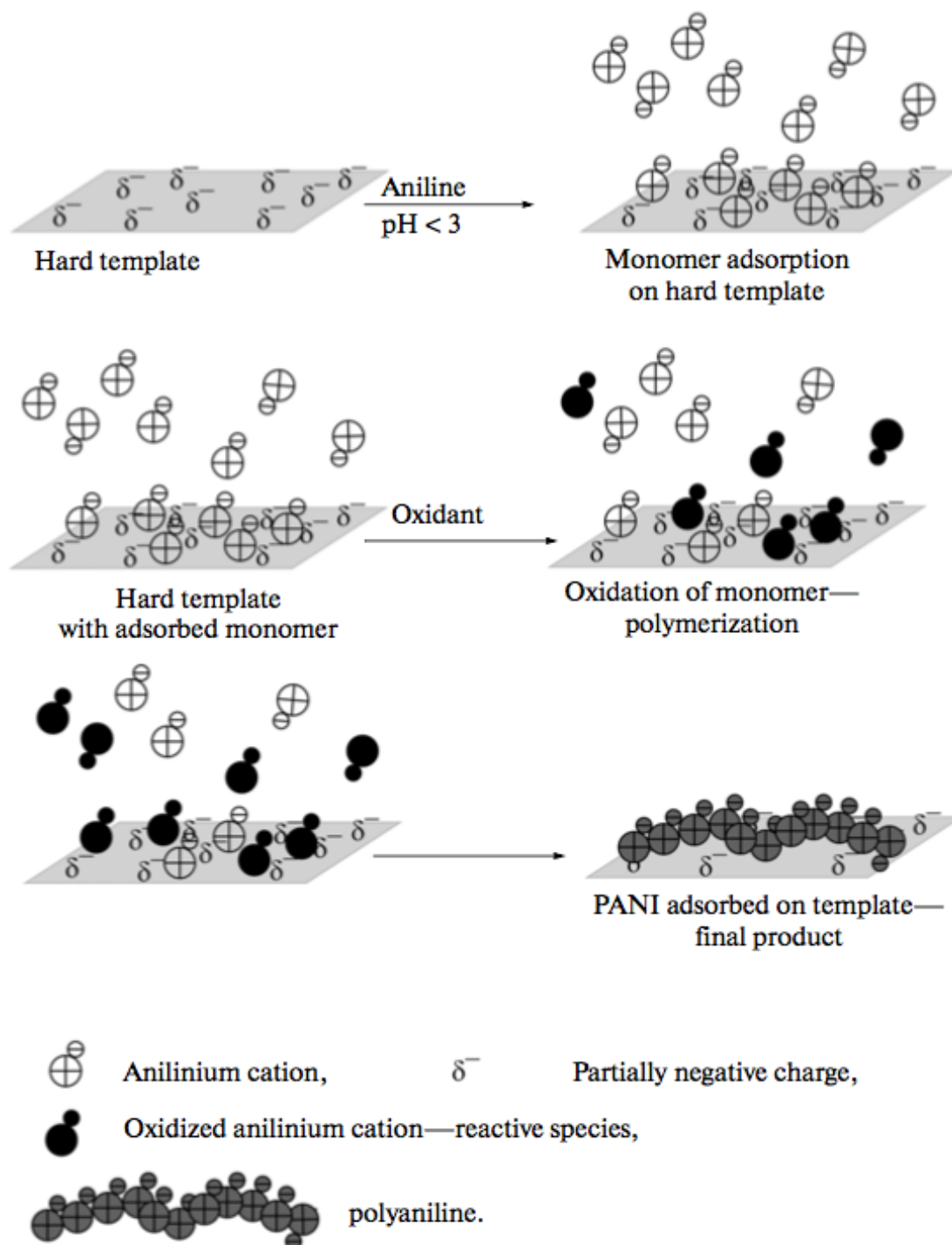


Figure 2.13 Overview of electrochemical polymerisation of aniline on substrate [16].

2.5.4 Properties of polyaniline

PANI has unique properties that preferable than other CPs such as switching, optical, conductive, and solubility properties [7].

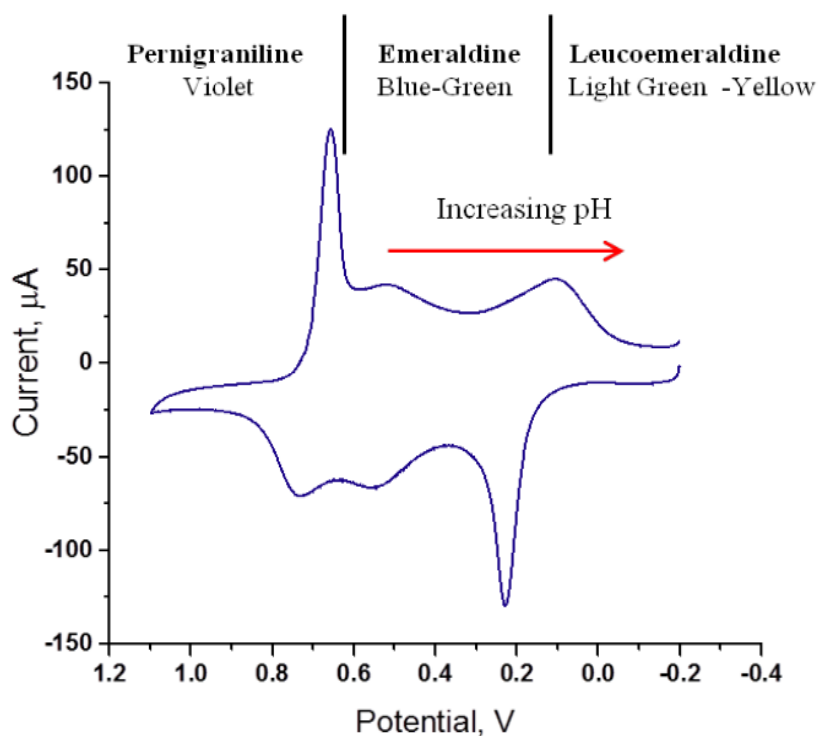


Figure 2.14 Cyclic voltammogram of PANI film on a Pt electrode in 1 M HCl at a scan rate 0.1 V s^{-1} . (The potentials at which structure and colour changes occur and the change in the potential of the second redox reaction with pH are shown as well) [7].

The switching and optical properties of PANI are related and influence each other directly [7]. The oxidation state of PANI can switching by addition of an acid or a base to protonates or deprotonates at the base (-NH-) sites of PANI due to the oxidation state of PANI depend on pH parameter [7]. As show in **Figure 2.14**, the electrochemical switching of PANI between oxidation states can be determined by cyclic voltammetry, which shows the trend of PANI structural switching with pH and redox potentials [7]. The electronic band gap of the various PANI structures can calculate from absorbance parameters due to UV - visible spectrum of PANI is

responsive to oxidation state and transitions between oxidation states [7]. Hence, the absorbance characteristics are related to the unique transitions which occur during the switching between oxidation states of PANI [7].

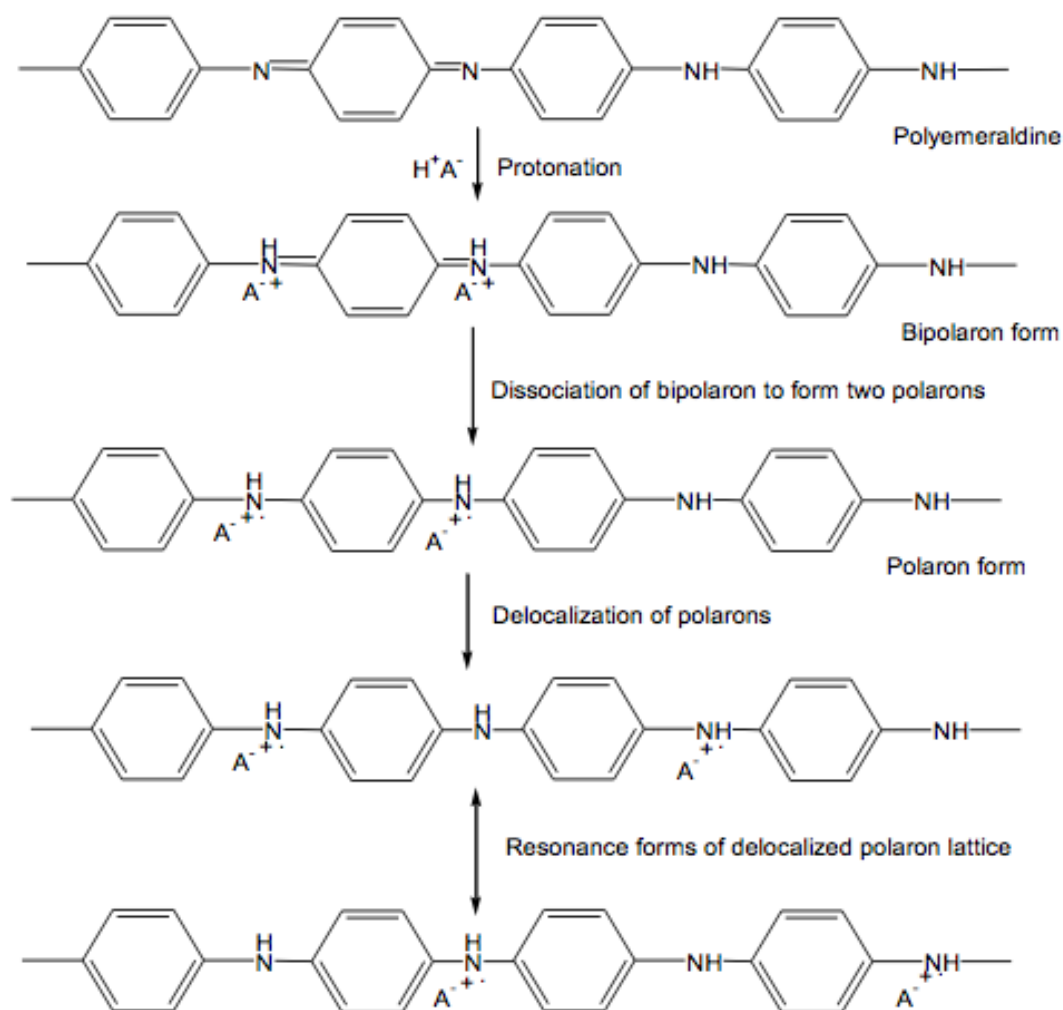


Figure 2.15 The doping of EB with protons to form the conducting emeraldine salt (PANI/HA) form of PANI (a polaron lattice) [7].

The conductivity properties of PANI depend on the extent of oxidation (variation in the number of electrons) and the degree of protonation (variation in the number of protons) [7]. In the various oxidation states of PANI, the emeraldine base is a remarkable state that can be modified to obtain a highly conductive state due to emeraldine base has a mixed structure that consists of amines ($-NH-$) and imine

(=N⁻) sites [7]. As show in **Figure 2.15**, the imine sites of emeraldine base was protonated by acids to the bipolaron (dication salt) form and then it was rearrangement to form the delocalized polaron lattice which is a polysemiquinone radical-cation salt [7]. Moreover, the conductivity of emeraldine salt on a semiconductor level has the order of 100 S cm^{-1} that is many orders of magnitude higher than the common polymers ($<10^{-9} \text{ S cm}^{-1}$) but lower than the common metals ($>10^4 \text{ S cm}^{-1}$) [7].

The solubility properties of PANI in emeraldine base state is insoluble in aqueous solution but it is soluble in a various organic solvent such as dimethyl sulfoxide, chloroform, tetrahydrofuran, dimethyl formamide, and methyl pyrrolidinone because emeraldine base is an oxidation state of PANI that does not have cationic charges in the polymer backbone [7]. Although, the emeraldine salt has cationic charges in the polymer backbone but it still insoluble in aqueous solutions and typical organic solvents [7]. The solubility of emeraldine state can be improved by addition of sulfonic acid derivatives as a dopant such as 10-champhor sulfonic acid, dodecyl-benzene sulfonic acid, poly(2-methoxyaniline-5-sulfonic acid) (PMAS), and polyaniline naphthathelene sulfonic acid (PANSA) [7].

2.6 Titanium dioxide

Titanium dioxide (TiO₂) or titania is a metal oxides semiconductor, which is a distinctive n-type material due to the Titanium-iron oxide mineral (FeTiO₃) or ilmenite is the mostly source of TiO₂ [17]. TiO₂ has band gap (E_g) slightly above 3.0 eV, which the three crystal structures of TiO₂ including anatase = 3.4 eV, rutile = 3.0 eV, and brookite = 3.3 eV, and reflective index (n) = 2.5 [18]. TiO₂ has a several applications such as paints, fabrics, plastics, cosmetics, and PV cell. Moreover, it has high optical and thermal stability, low toxicity, environmental green, less expensive, corrosion resistance, and ease of synthesis [1]. It was a suitable material for applied OPV cells.

2.6.1 TiO₂ nanorods

The TiO₂ nanorods have a remarkable advantage such as a direct pathway for electron transfer with fewer grain boundaries due to the existence of a continuous

wall, the vectorial electron transport without significant losses as shown in **Figure 2.16 (a)**, and high light absorption due to the light trapping effect [3].

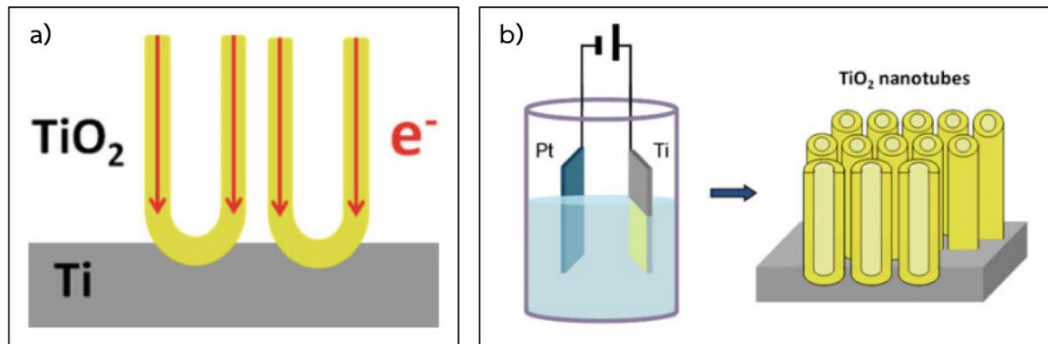


Figure 2.16 (a) The vectorial electron transport along the nanotubes axis and **(b)** the electrochemical cell of TiO_2 nanorods synthesis [17].

The TiO_2 nanorods can synthesize by electrochemical anodic oxidation (anodization) of titanium in a fluoride-based electrolyte, which has three generations [17]. In the first-generation using HF acid water-based solution as an electrolyte, but the thickness of TiO_2 nanorods were limited to hundreds of nanometers due to HF is a strong acid that highly corrosive to nanorods structure. The second-generation, the thickness of TiO_2 nanorods increased into micrometers by using buffered neutral electrolytes which consisted the fluoride compound such as sodium fluoride (NaF), potassium fluoride (KF), and ammonium fluoride (NH_4F) instead of HF. And the third-generation, the thickness of TiO_2 nanorods increased into 1 mm and a variety of morphologies such as single wall, double wall, multilayer, and branched nanorods by using the fluoride compound as a supporting electrolyte in the organic solution that is mainly ethylene glycol and the co-solvent H_2O as an electrolyte solution. The electrochemical anodization of titanium was consisting of the electrolyte, the working electrode using as an anode, the counter electrode using as a cathode, and the external source that has two methods including potentiostatic oxidation (constant potential) and galvanostatic oxidation (constant current) as shown in **Figure 2.16 (b)** [17].

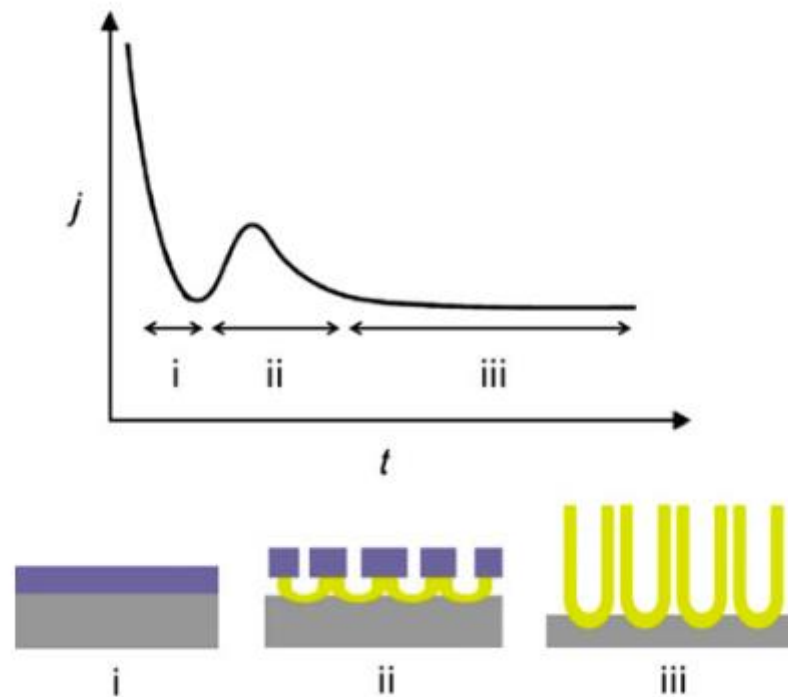
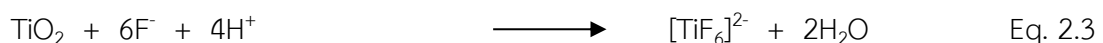
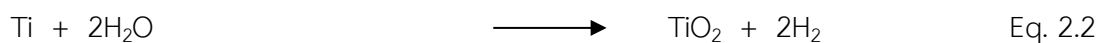
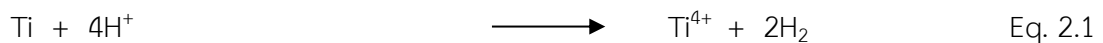


Figure 2.17 The three stages of TiO_2 nanorods potentiostatic anodization and the corresponding current density - time (j - t) diagram [17].

The TiO_2 nanorods potentiostatic anodization has three main stages as shown in **Figure 2.17**. Firstly, the initial stage (i) is the formation step of TiO_2 compact on Ti surface. The second stage (ii), the fluoride ion in electrolyte was penetrated through weak points on TiO_2 compact and start to growth porous tubular layer at TiO_2/Ti interface. The final stage (iii), TiO_2 nanorods were continued growth, while TiO_2 compact was peeling off at constant current or voltage [17].



The chemical reactions during electrochemical anodization of titanium in a fluoride-based electrolyte were shown in Eq. 2.1 – 2.3 [17]. The Eq. 2.1 is summary reactions between the Ti metal oxidation on working electrode or anode to oxidized

Ti metal into Ti^{4+} and hydrogen ions reduction to released H_2 gas on counter electrode or cathode [17]. TiO_2 nanorods can be generated by a balance between the TiO_2 formation at oxide/metal interface (Eq. 2.2) and the oxide dissolution at electrolyte/oxide interface (Eq. 2.3) [17]. If the dissolution rate higher than the growth rate, Ti and TiO_2 are soluble in an electrolyte solution and the cell at the anode was corrosion, whereas the dissolution rate is too small, not enough to peel off the TiO_2 compact layer from the TiO_2 nanorods [17].



CHAPTER 3

LITERATURE REVIEWS

3.1 Comparison of photovoltaic properties between PANI and PEDOT:PSS

Poly (3,4-ethylenedioxythiophene):poly (styrenesulfonate) (PEDOT:PSS) and PANI has been a pi-conjugated polymer that has a transparent conductive ability and both of them suitable for use as a p-type material for PV applications [5].

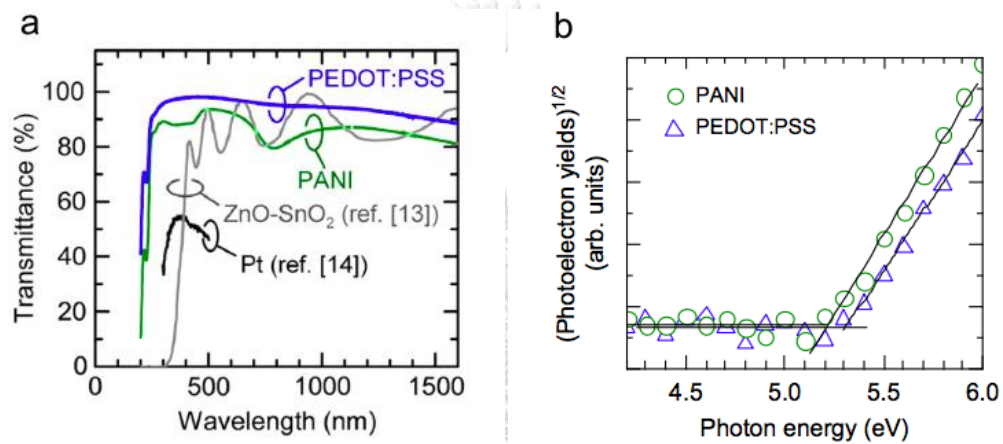


Figure 18 (a) Optical transmittance spectra of PEDOT:PSS and PANI films and (b) Photoelectron emission spectra of PEDOT:PSS and PANI films [5].

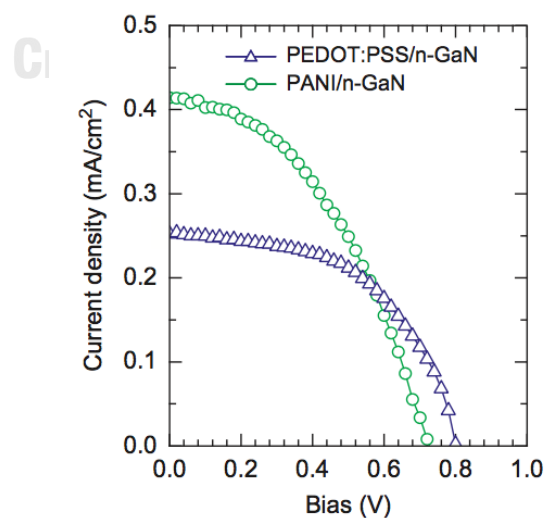


Figure 19 The PV characteristics of PEDOT:PSS/n-GaN/sapphire (0 0 0 1) and PANI/n-GaN/sapphire (0 0 0 1) samples under AM1.5 light irradiation [5].

The optical transmittance spectra of the PEDOT:PSS and PANI films exhibited more than 80% of transmittance, which is more than conventional transparent contact materials, within the wavelength region 250 to 1500 nm that show in **Figure 3.1 (a)** [5]. The Photoelectron emission spectra of the PEDOT:PSS and PANI films are found photon energy to be 5.3 and 5.2 eV that show in **Figure 3.1 (b)** indicate that the photoelectron emission of PANI using less light energy than PEDOT:PSS to generate photoelectron [5].

The PV performances of PANI/n-GaN/sapp (0 0 0 1) and PEDOT:PSS/n-GaN/sapp (0 0 0 1) samples such as open-circuit voltage (V_{oc}) = 0.73 and 0.80 V, short-circuit current density (J_{sc}) = 0.41 and 0.25 mA/cm², maximum output power (P_{max}) = 0.13 and 0.11 mW/cm², and the fill factor (FF) = 0.42 and 0.54 [5]. All of the resulting values can be estimated from the PV characteristics (J–V measurements under AM1.5 light irradiation) show in **Figure 3.2** that indicate PANI/n-GaN/sapp (0 0 0 1) can be generate current in the system more than PEDOT:PSS/n-GaN/sapp (0 0 0 1) [5].

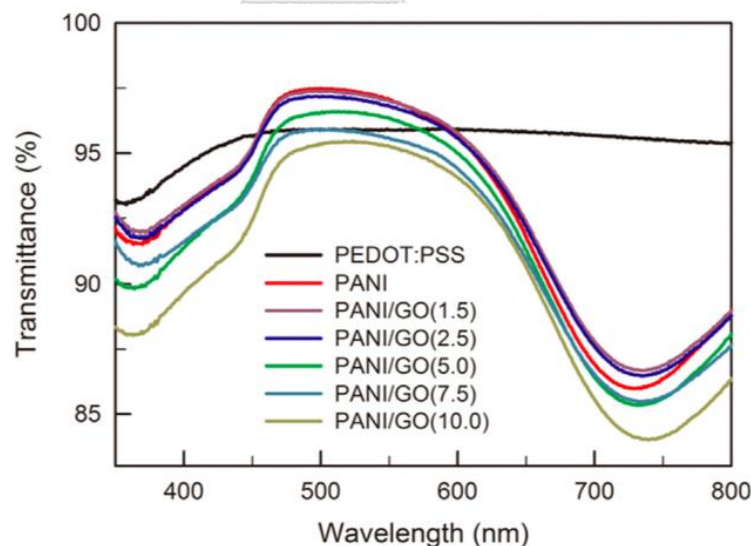


Figure 20 Transmittances of PEDOT:PSS, PSSA-g-PANI and PSSA-g-PANI/GO composite films, where the film thickness is 40 nm [6].

The transmittance spectra of PANI and PEDOT:PSS films were found to be 97.1% and 95.9%, respectively that show in figure 3.3 indicate that PANI films exhibit transmitted than PEDOT:PSS films, which both films had a thickness of 40 nm [6].

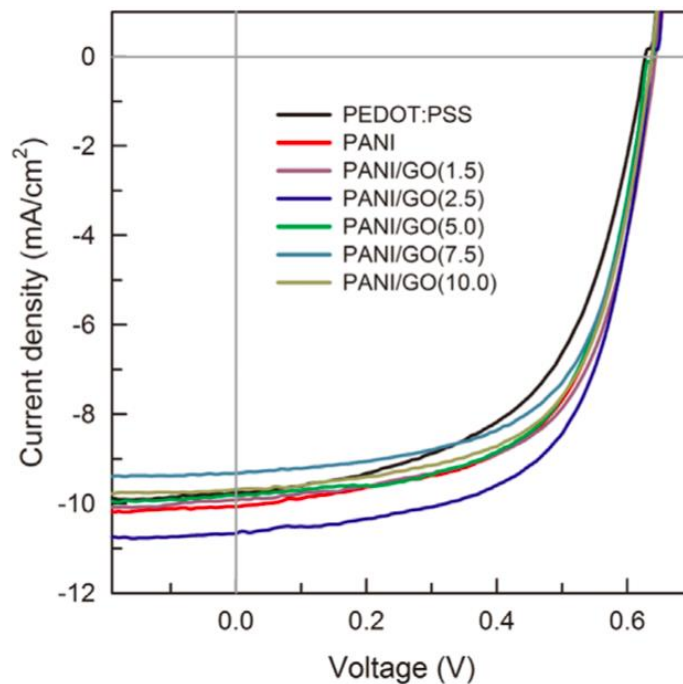


Figure 21 The J-V curves measured under AM 1.5 G (100 mW/cm^2) of P3HT:P₆₁BM PV cell with PEDOT:PSS, PSSA-g-PANI, and PSSA-g-PANI/GO composites as HTL [6].

The J-V curves of PV cells with PANI and PEDOT:PSS as hole transport layer (HTL) are shown in **Figure 3.4** that can be calculate the PV performances such as the short-circuit current density (J_{SC}), open-circuit voltage (V_{OC}), fill factor (FF) and power conversion efficiency (PCE) values [6]. The result shows PV cells with PANI exhibit higher J_{SC} and higher PCE than PV cells with PEDOT:PSS which, indicated PV cells with PANI has higher optical transmittance, higher electrical conductivity and higher hole transport performance as compared to PV cells with PEDOT:PSS [6]. However, several drawbacks of PEDOT:PSS have been reported such as large particle size of 60 - 80 nm, strong acidic nature of PSS, high cost and low electrical conductivity [6]. Although PANI and PEDOT: PSS have very similar properties, the difference is that PANI's price is cheaper which, is why PANI was interested in this research.

3.2 Electrochemical polymerisation of polyaniline on substrate

Tan, F. (2013) has purpose electropolymerisation method operate with constant potential at 1.20 V for 180 s to deposited 9-anthracene methyl acid (AMA) : PANI on ITO/glass substrates [15]. The component of an electrolyte solution was composed of 10 mL ethanol and 0.1 mL aniline ($C_6H_5NH_2$) [15]. The mole ratio (AMA : aniline) was varying into 1:4, 1:2 and 1:1, respectively, and the PANI without AMA doping were operated under the same condition method [15]. The Ag/AgCl electrode, a platinum net, and the ITO glass substrates were served as the reference electrode (RE), the counter electrode (CE) and the working electrode (WE), respectively, the three electrodes were set up for electropolymerisation [15].

Gizzie, E. A. (2015) has purpose electropolymerisation method operate with constant potential at +6.50 V for 120 s to deposited PANI-PSI films on TiO_2 /FTO substrates glass, which was performed by using a CH Instruments 660A potentiostat [19]. The component of an aqueous electrolyte solution for synthesis was composed of 1 M $C_6H_5NH_2$, 0.94 M HCl, 4 mM sodium phosphate (Na_3PO_4), and 1.3 μ M PSI that was extracted and purified from commercial spinach leaves (*Spinacia oleracea*) [19]. The Ag/AgCl (3 M KCl) electrode, a platinum mesh, and the TiO_2 /FTO glass substrates were served as RE, CE and WE, respectively, the three electrodes were set up for PANI-PSI electrodeposition [19].

Budi, S. (2020) has purpose electropolymerisation method operate with constant potential at +0.5 V for 5 min to deposited PANI on stainless steel as substrate, which was performed by using an Edaq EA 163 potentiostat [20]. The component of electrolyte solution was composed of 0.5 M aniline ($C_6H_5NH_2$) and 0.5 M H_2SO_4 [20]. The Ag/AgCl electrode, a platinum, and a stainless steel were served as RE, CE and WE, respectively, the three electrodes were set up for PANI electropolymerisation [20].

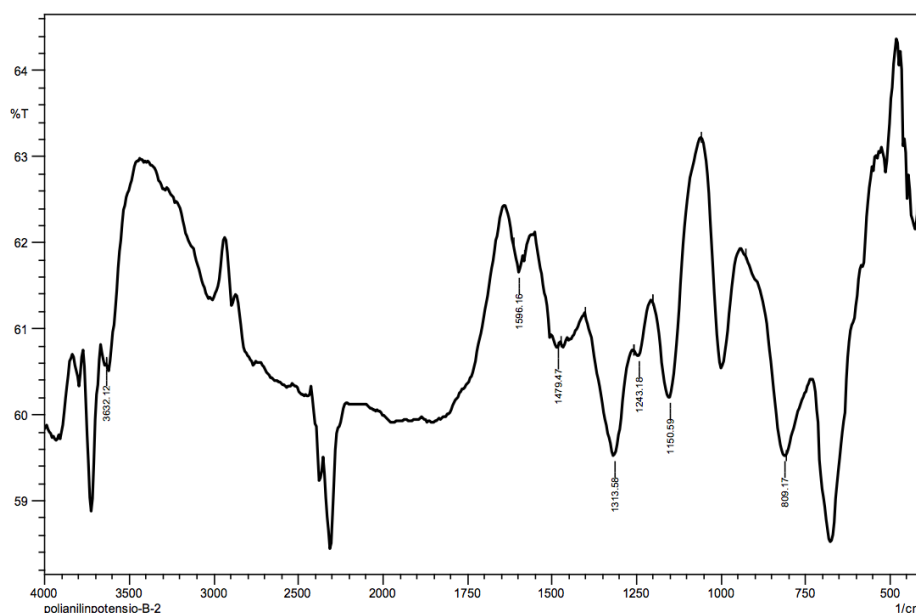


Figure 22 IR spectrum of PANI that synthesis by electropolymerisation method with constant potential at +0.5 V for 5 min [20].

The molecular structure of polymerized PANI on stainless steel was determined by FTIR spectra between 4000 - 400 cm^{-1} . As show in **Figure 3.5** the IR spectrum of PANI had many peaks that corresponding to functional groups including a peak at 3632.12 cm^{-1} (asymmetric N-H stretching), 2250 - 2500 cm^{-1} (aromatic C-H sp^3 stretching in a benzenoid group), 1596.16 cm^{-1} (C=C vibration in a quinoid group), 1479.47 cm^{-1} (aromatic C=C stretching in a benzenoid group), 1313.58 cm^{-1} (C-N stretching in a benzenoid ring), 1150.59 cm^{-1} (C-N stretching in a quinoid ring), and 809.17 cm^{-1} (out-of-plane C-H bending in a 1,4-disubstituted benzene ring) [20]. According to all of IR spectrum indicate that the molecular structure of polymerized PANI is an emeraldine base, which is a partially oxidized and partially reduced emeraldine state consists both of benzenoid and quinonoid units.

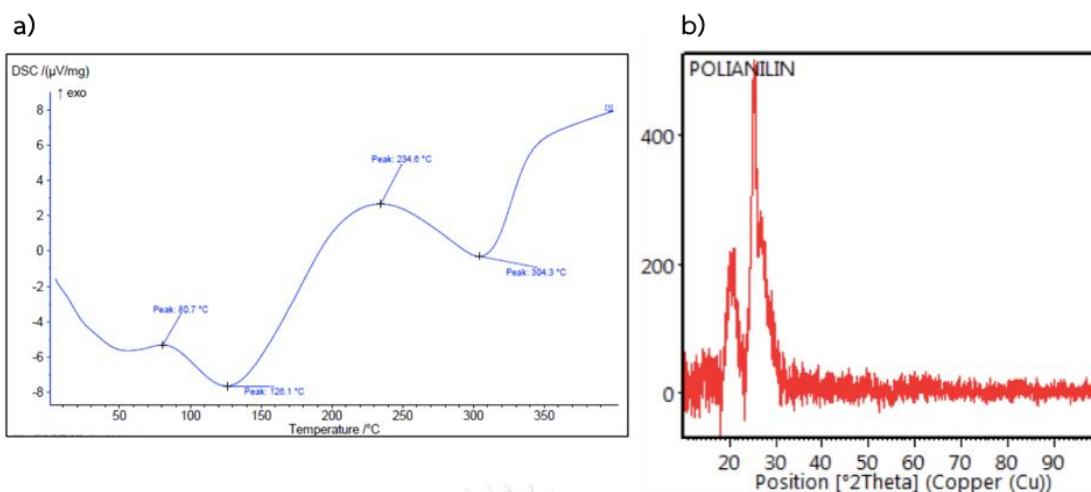


Figure 23 (a) DSC thermogram and **(b)** Diffraction pattern of PANI that synthesis by electropolymerisation method with constant potential at +0.5 V for 5 min [20].

As show in **Figure 3.6 (a)**, the DSC thermogram of PANI had four peaks including three endothermic peaks and an exothermic peak [20]. The endothermic peaks were observed at 80.7, 126.1, and 304.3°C corresponding to the glass transition temperature at which the rigid solid changed into plastic form, the elimination of H₂O molecules and impurities trapped in PANI films, and the melting point of PANI, respectively [20]. The exothermic peak was observed at 234.6°C corresponding to an irreversible reaction of oxidation and/or a cross-linking of polymers and the crystallization of PANI can occur at this temperature [20]. The diffraction pattern of PANI were show in **Figure 3.6 (b)** that consisted of two diffraction peaks at $2\theta = 21.488^\circ$ and 25.295° corresponding to the forms of PANI consisted of quinoid and benzenoid units, which is this diffraction pattern of a semi-crystalline form due to the peak at $2\theta = 21.488^\circ$ is characteristic of PANI, while 25.295° is the part of a sub-chain from PANI became rigid and well-arranged [20].

3.3 Morphology of Polyaniline

Budi, S. (2020) has shown *Figure 3.7*, which is a SEM image of PANI that synthesized by electropolymerisation method [20]. The morphology of PANI was composed of 0.2 μm diameter fibers, which agglomerated in non-uniform with a disorder manner [20].

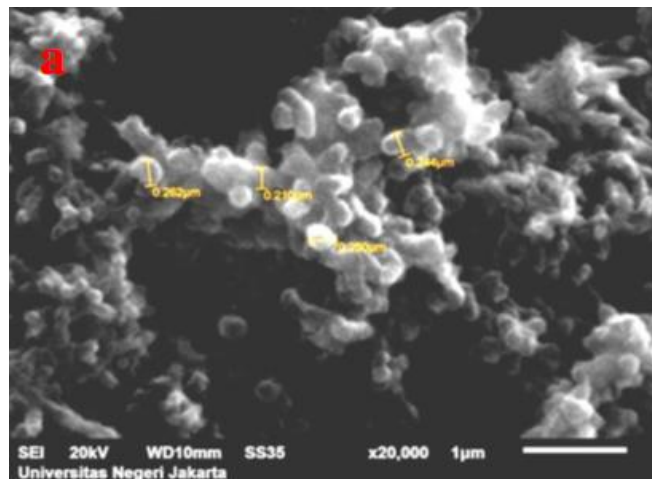


Figure 24 SEM images of PANI that synthesized by Budi, S. (2020) electropolymerisation method [20].

Karami, H. (2012) has purpose electropolymerisation method operate with pulse current density (pulse galvanostatic) to synthesized PANI nanopowder filled in the porous graphite electrode, which was performed by using an Autolab (Eco Chimie, PGSTAT-10) [21].

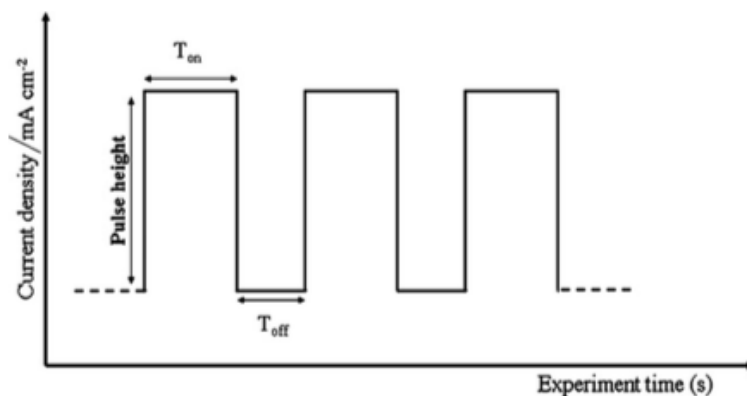


Figure 25 The pulse current density diagram [21].

The component of an aqueous electrolyte solution for synthesis was composed of $C_6H_5NH_2$ and perchloric acid ($HClO_4$) [21]. The Ag/AgCl electrode, a platinum electrode, and the porous graphite electrode were served as RE, CE, and WE, respectively, the three electrodes were set up for PANI electrodeposition [21]. In Karami, H. (2012) research, the parameters including the pulse current densities, relaxation times (t_{off}), pulse times (t_{on}), temperatures, aniline concentrations, and perchloric acid concentrations were varying to observe PANI morphology.

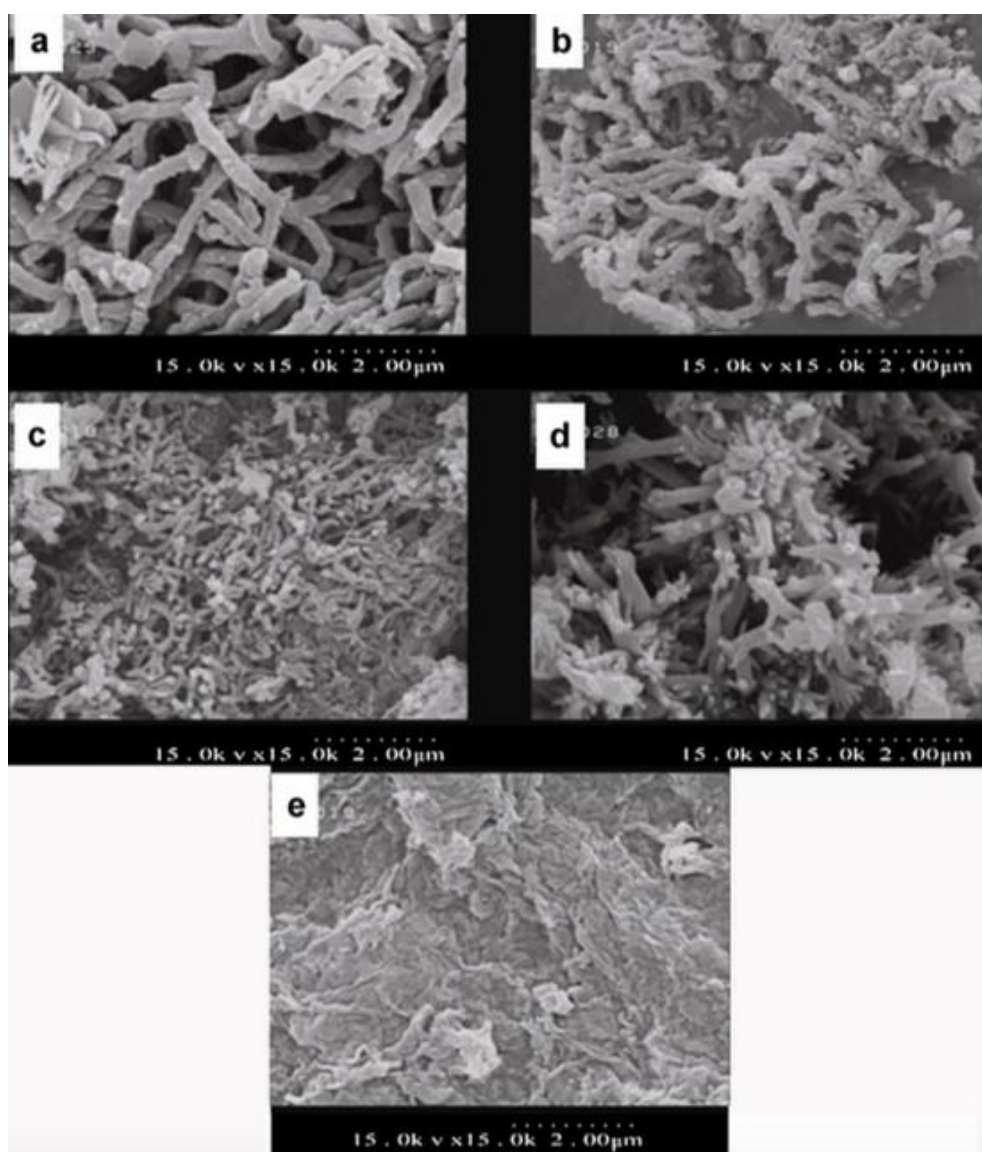


Figure 26 SEM images of PANI with the different pulsed current densities: (a) 10 mA cm^{-2} , (b) 30 mA cm^{-2} , (c) 75 mA cm^{-2} , (d) 125 mA cm^{-2} , and (e) 200 mA cm^{-2} [21].

To observe the effect of pulsed current density parameter, the parameters including temperature, aniline concentration, perchloric acid concentration, t_{on} , and t_{off} were kept constant at 25 °C, 0.1 M $C_6H_5NH_2$, 1.0 M $HClO_4$, 0.5 s, and 0.5 s, respectively, and the pulsed current densities were varied from 10, 30, 75, 125, and 200 $mA\ cm^{-2}$ [21]. The increasing of pulsed current density parameter will affect more amorphous form; on the other hand, if the pulsed current density parameter was decreased from 200 to 10 $mA\ cm^{-2}$ shift to more fiber uniform as shown in **Figure 3.9** [21]. The pulsed current density 10 $mA\ cm^{-2}$ is more fiber uniform with smaller diameters and longer lengths than high pulsed current density [21].

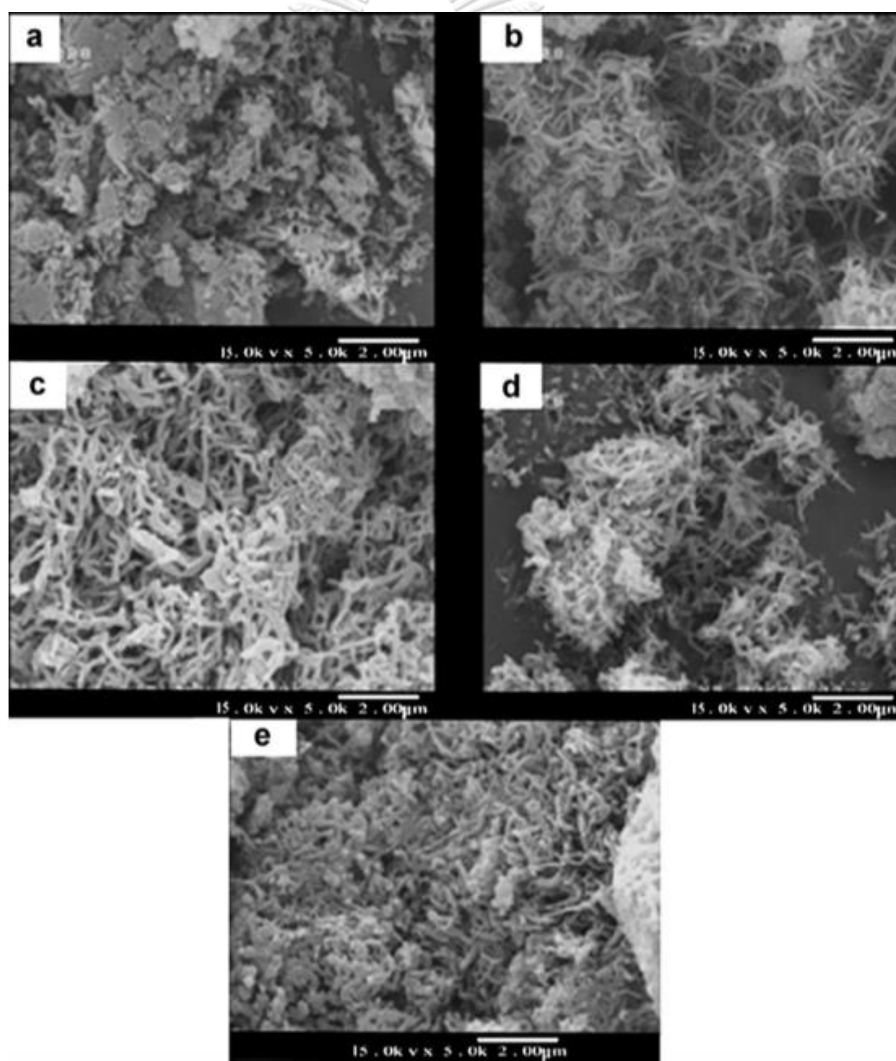


Figure 27 SEM images of PANI with the different relaxation times (t_{off}): (a) 0 s, (b) 0.25 s, (c) 0.5 s, (d) 1.0 s, and (e) 2.0 s [21].

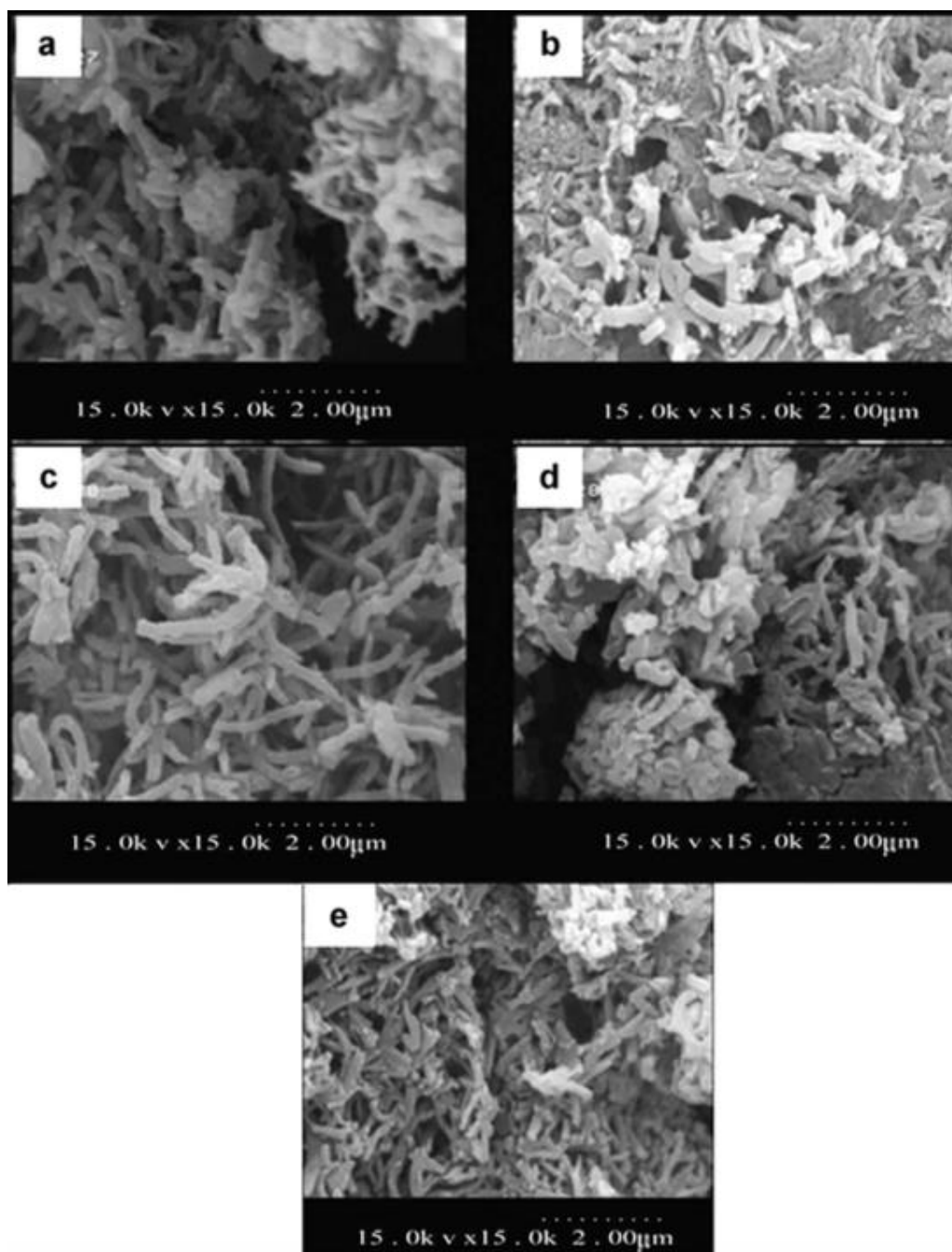


Figure 28 SEM images of PANI with the different pulse times (t_{on}): (a) 0.1 s, (b) 0.25 s, (c) 0.5 s, (d) 1.0 s, and (e) 2.0 s [21].

The effect of relaxation time parameter and the effect of pulse time parameter can observe by kept constant of the parameters including the pulsed current density, temperature, aniline concentration, and perchloric acid concentration at 10 mA cm^{-2} , $25 \text{ }^\circ\text{C}$, $0.1 \text{ M C}_6\text{H}_5\text{NH}_2$, and 0.1 M HClO_4 , respectively,

and kept constant of pulse time at 0.5 s to observe the effect of relaxation time by varying relaxation times: 0, 0.25, 0.5, 1.0, and 2.0 s [21]. As shown in *Figure 3.10*, the optimized relaxation time is 0.25 s due to it was more fibers uniform and smaller diameters than 0, 0.5, 1.0, and 2.0 s of relaxation times [21]. To observe the effect of pulse time by kept constant of relaxation time at 0.25 s and varying relaxation times: 0.1, 0.25, 0.5, 1.0, and 2.0 s [21]. As shown in *Figure 3.11*, the optimized pulse time is 0.5 s due to it was more fibers uniform and smaller diameters than 0.1, 0.5, 1.0, and 2.0 s of pulse times [21].

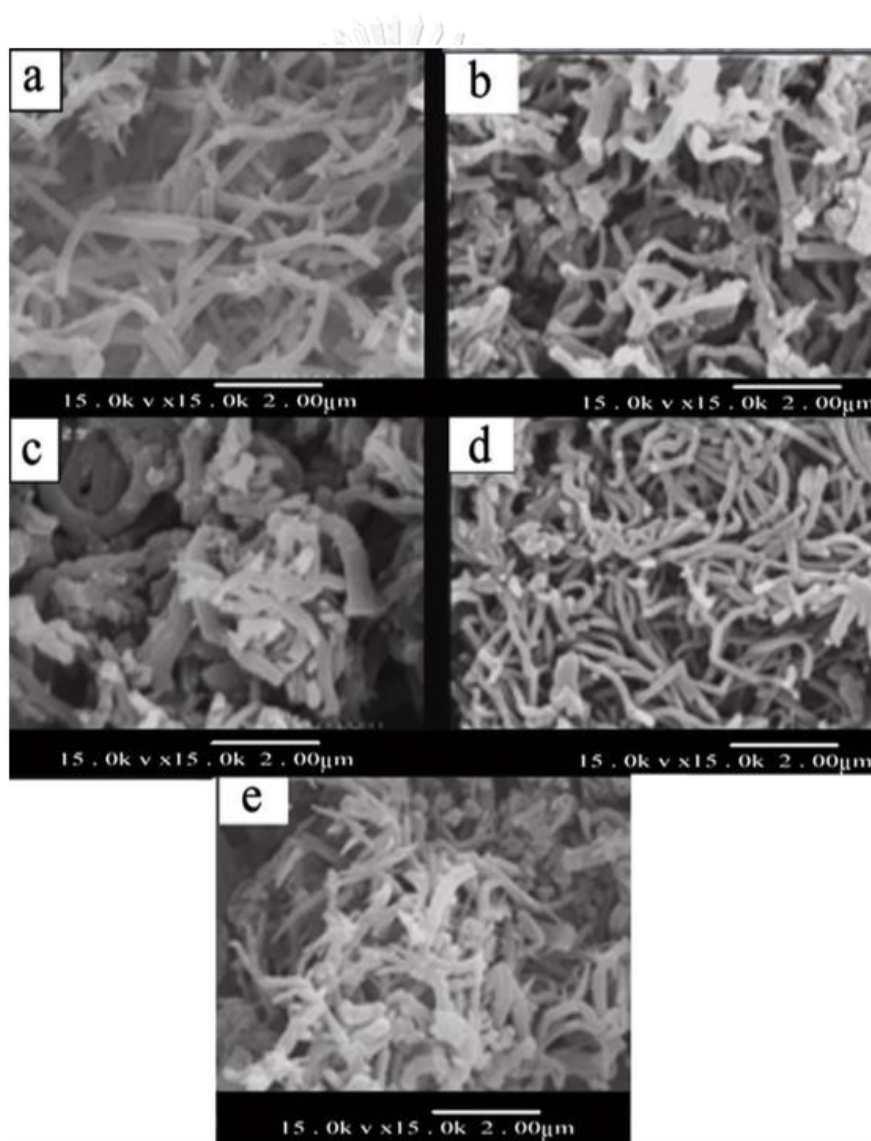


Figure 29 SEM images of PANI with the different temperatures (a) 15 °C, (b) 25 °C, (c) 35 °C, (d) 45 °C, and (e) 55 °C [21].

To observe the effect of temperature parameter, the parameters including pulsed current density, aniline concentration, perchloric acid concentration, t_{on} , and t_{off} were kept constant at 10 mA cm^{-2} , $0.1 \text{ M C}_6\text{H}_5\text{NH}_2$, 1.0 M HClO_4 , 0.5 s , and 0.25 s , respectively, and the temperatures were varied from 15 , 25 , 35 , 45 , and $55 \text{ }^\circ\text{C}$ [21]. As shown in **Figure 3.12**, the optimized temperature is $45 \text{ }^\circ\text{C}$ due to it was more fibers uniform and smaller diameters than 15 , 25 , 35 and $55 \text{ }^\circ\text{C}$ of temperature [21].

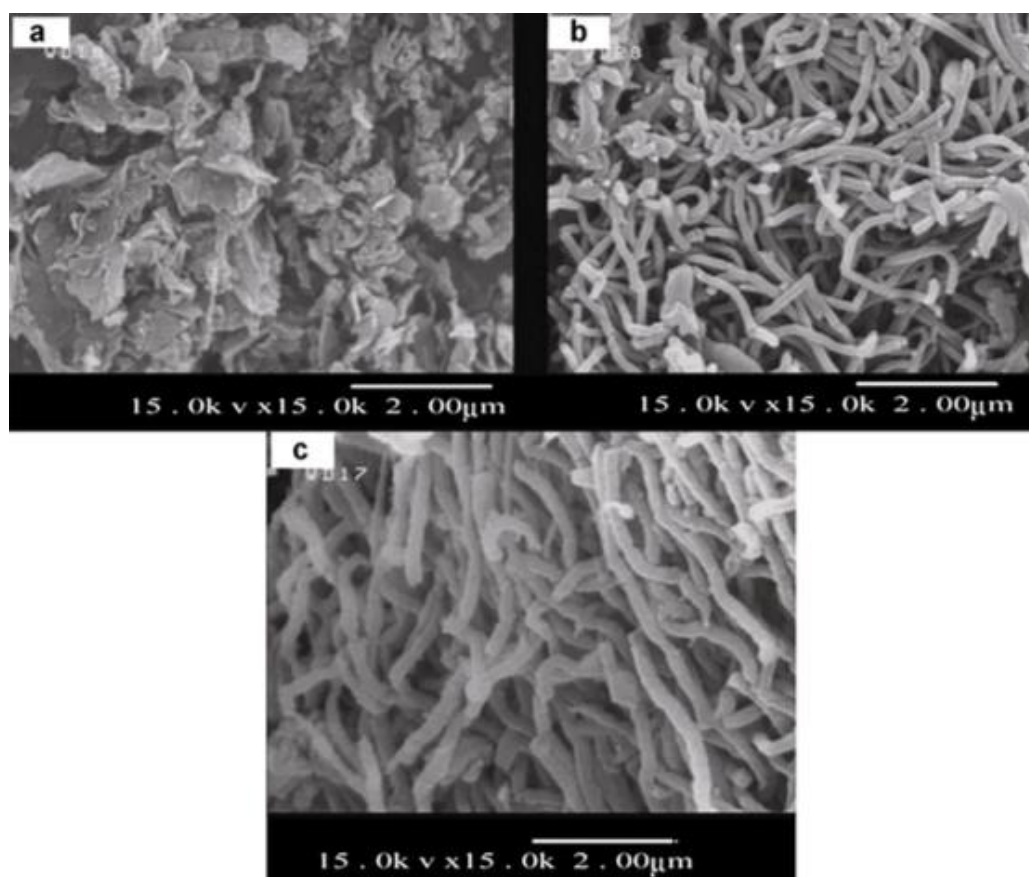


Figure 30 SEM images of PANI with the different aniline concentrations: (a) 0.05 M , (b) 0.1 M , and (c) 1.0 M [21].

The effect of aniline concentration parameter can observe by kept constant of the parameters including the pulsed current density, temperature, perchloric acid concentration, t_{on} , and t_{off} at 10 mA cm^{-2} , $45 \text{ }^\circ\text{C}$, 1.0 M HClO_4 , 0.5 s , and 0.25 s , respectively, and the aniline concentrations were varied from 0.05 , 0.1 , and 1.0 M [21]. As shown in **Figure 3.13**, the most fiber uniform of PANI is $0.1 \text{ M C}_6\text{H}_5\text{NH}_2$ and diameter of $0.1 \text{ M C}_6\text{H}_5\text{NH}_2$ is smaller than $1.0 \text{ M C}_6\text{H}_5\text{NH}_2$ [21].

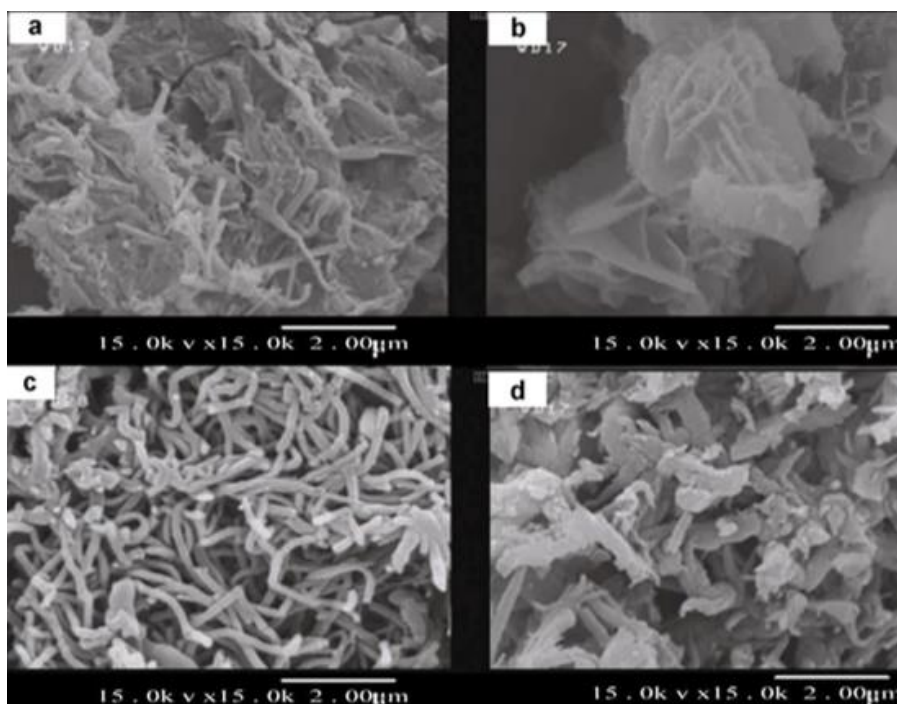


Figure 31 SEM images of PANI with the different perchloric acid concentrations: **(a)** 0.05 M, **(b)** 0.1 M, **(c)** 1.0 M, and **(d)** 2.0 M [21].

The effect of perchloric acid concentration can observe by kept constant of the parameters including the pulsed current density, temperature, aniline concentration, t_{on} , and t_{off} at 10 mA cm^{-2} , $45 \text{ }^\circ\text{C}$, $0.1 \text{ M C}_6\text{H}_5\text{NH}_2$, 0.5 s , and 0.25 s , respectively, and the perchloric acid concentrations were varied from 0.05, 0.1, 1.0, and 2.0 M [21]. the most fiber uniform of PANI is 1.0 M HClO_4 was shown in **Figure 3.14** [21].

3.4 Polyaniline in photovoltaic cells

Tan, F. (2013) synthesized an AMA : PANI thin films with the different in the mole of AMA doping by electropolymerisation method [15]. In general, undoped PANI or 0:1 of AMA : PANI films (leucoemeraldine state) exhibit as an inferior electroconductivity insulator [15]. **Figure 3.15 (a)** shows the absorption spectra of AMA : PANI thin films with the different in the mole of AMA doping and incident photon energy indicate that the optical band gap of the doped PANI films were decreases when the mole of AMA was increasing, which improve the electroconductivity of thin films [15].

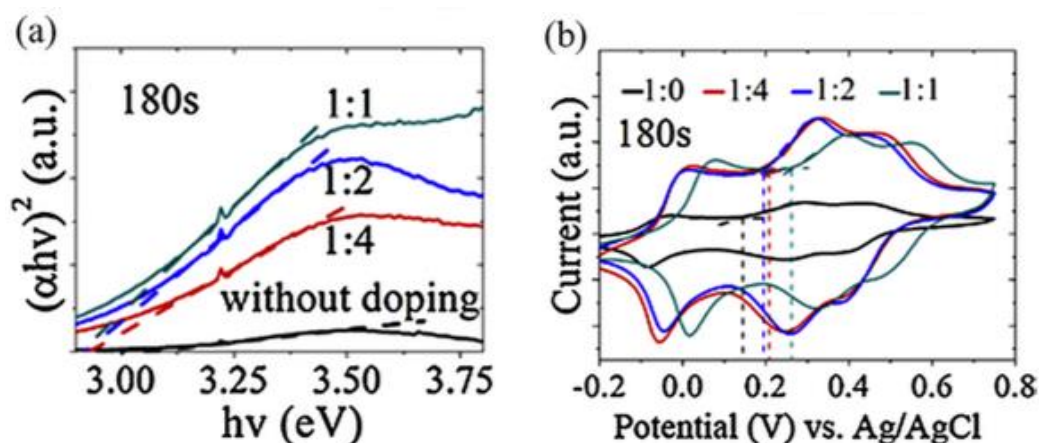


Figure 32 (a) Light absorption and (b) CV characterization of PANI films with the different doping ratios [15].

The CV characterization of AMA : PANI thin films with a difference in the mole of PANI were shown in **Figure 3.15 (b)** [15]. The three redox peaks of 1:4, 1:2, and 1:1 (AMA : PANI) in accordance with the different oxidation states, which observed the onset of the oxidation peak of 1:1 (AMA : PANI) is slightly shifted to a higher potential than the ratio of 1:4 and 1:2 (AMA : PANI) due to the AMA doping ratio is increased that probably caused by the withdrawing of electrons to AMA chain and its influence on the coplanarity of the PANI molecules [15].

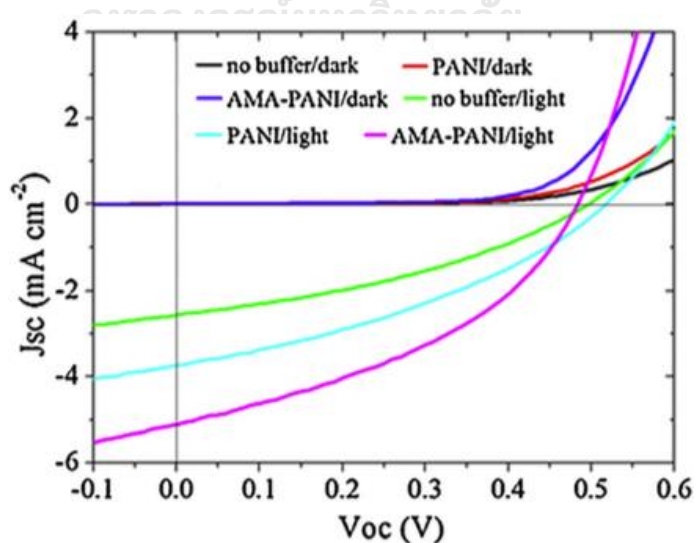


Figure 33 The J-V curves of device with the different PANI films as anode buffer layers devices tested in the dark and under 100 mW cm^{-2} illumination [15].

The PV performance of AMA : PANI thin films, were perform in the dark and under 100 mW cm^{-2} illumination, that using as anode buffer layer shows in **Figure 3.16** that can calculate to obtain J_{SC} value of 1:4, 1:2, and 1:1 (AMA : PANI) is 4.6 , 5.0 , and 4.8 mA cm^{-2} , respectively, which is not significantly different but compared with undoped PANI film as the buffer layer ($J_{SC} = 3.8 \text{ mA cm}^{-2}$) and PV cell without buffer layer ($J_{SC} = 2.6 \text{ mA cm}^{-2}$), AMA doped PANI films were shown improve of PV performance [15]. However, the ratio 1:2 of AMA : PANI thin film was found to be the optimize mole ratio, that having the highest PV performance such as J_{SC} and the conversion efficiency (η) is 1.1% that higher than the PV cell with undoped PANI film ($\eta = 0.72\%$) and without buffer layer ($\eta = 0.45\%$) [15].

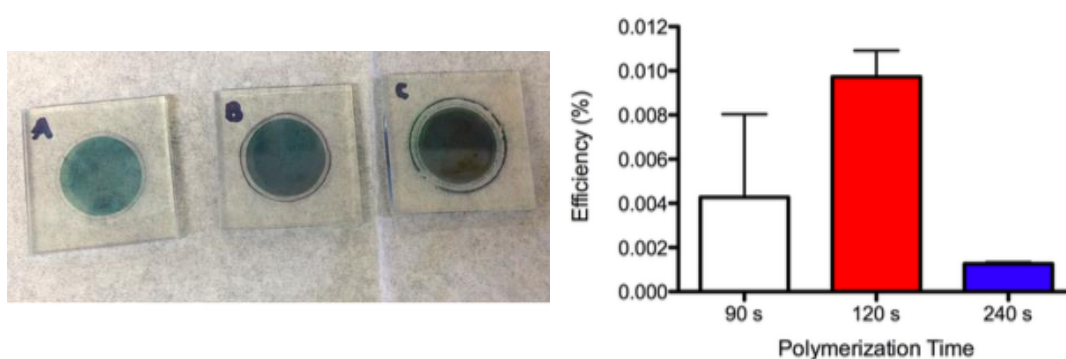


Figure 34 The images of PANi-PSI films deposited on $\text{TiO}_2/\text{FTO}/\text{glass}$ substrates. Samples were prepared from potentiostatic polymerisation at $+6.5 \text{ V}$, for A) 90, B) 120, and C) 240 s and the PV efficiency diagram of Ag/PANi-PSI/ TiO_2 PV cells prepared with active layer thicknesses polymerized for 90, 120, or 240 s [19].

Gizzie, E. A. (2015) synthesized a PANI-PSI thin films that exhibits as the p-type receptor semiconductor for biohybrid PV cell by electropolymerisation method [19]. Moreover, in this work was optimize the thicknesses to enhance photocurrent output of Ag/PANi-PSI/ TiO_2 and Ag/PANi-only/ TiO_2 solid-state PV cells by varying electropolymerisation times: 90, 120, and 240 s that shown in **Figure 3.17** [19]. The electropolymerisation time of 120 s has PV efficiency higher than 90 and 240 s indicate that the optimize thickness affect to the PV performance [19].

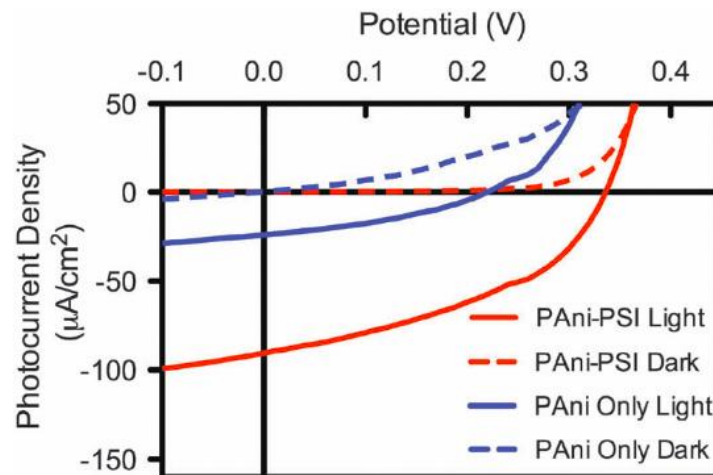


Figure 35 The I–V curves for Ag/PAni–PSI/TiO₂ and Ag/PAni-only/TiO₂ solid-state PV cells tested in the dark and under AM 1.5 solar simulated illumination [19].

The PV performance of Ag/PAni–PSI/TiO₂ and Ag/PAni-only/TiO₂ solid-state PV cells were tested in the dark and under AM 1.5 solar simulated illumination that shown in **Figure 3.18** [19]. The current density (J_{SC}) of Ag/PAni–PSI/TiO₂ and Ag/PAni-only/TiO₂ solid-state PV cells, which calculate from the gap between in the dark and under illumination at potential 0 V of each cell, were 72 and 21 $\mu\text{A cm}^{-2}$, respectively [19].

3.5 Synthesis of TiO₂ nanorods

Lee, B.-G. (2009) has purpose electrochemical anodization of titanium in a fluoride-based electrolyte method operate with constant potential 20 V for 60 min with the electrolyte solution that was composed of 1.5 wt% of NH₄F and the mixture of glycerin : D.I. water = 70 : 30 volume ratios to synthesized the TiO₂ nanorods [22]. The top and bottom view images of the synthesized TiO₂ nanorods, as shown in **Figure 3.19 (a)** and **(c)**, have shown the open tubes approximately 100 nm in diameter and the end tubes of the TiO₂ nanorods [22]. As shown in **Figure 3.19 (b)**, the cross-sectional view of the synthesized TiO₂ nanorods has shown the connected walls of the TiO₂ nanorods [22]. The synthesized TiO₂ nanorods with constant potential 20 V for 60 min and the electrolyte solution was composed of glycerin : D.I. water (70 : 30) without NH₄F was shown in **Figure 3.19 (d)**, which cannot observe

porous structure indicate that NH_4F was affected to porous structure formation in term of the dissolution reaction [22].

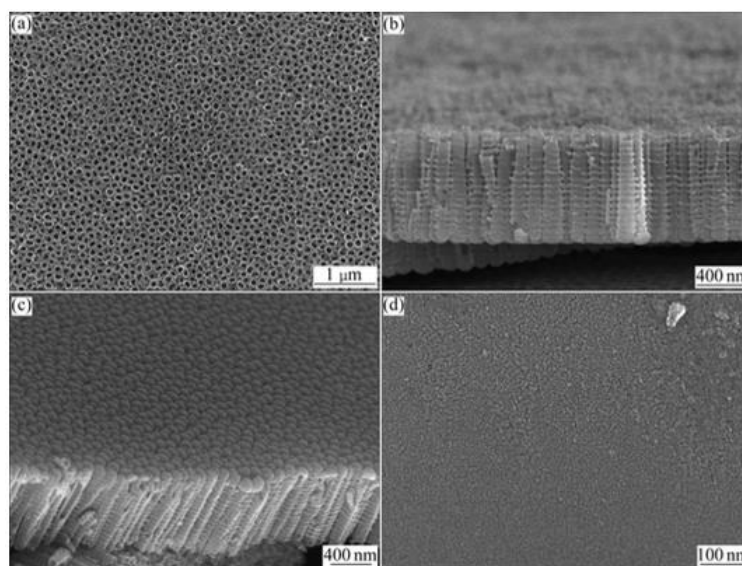


Figure 36 FE-SEM images of TiO_2 nanorods that anodized at 20 V for 60 min with 1.5% NH_4F and glycerin : D.I. water (70 : 30) electrolyte: (a) top view, (b) cross-sectional view, and (c) bottom view and (d) glycerin : D.I. water (70 : 30) without NH_4F electrolyte on top-view [22].

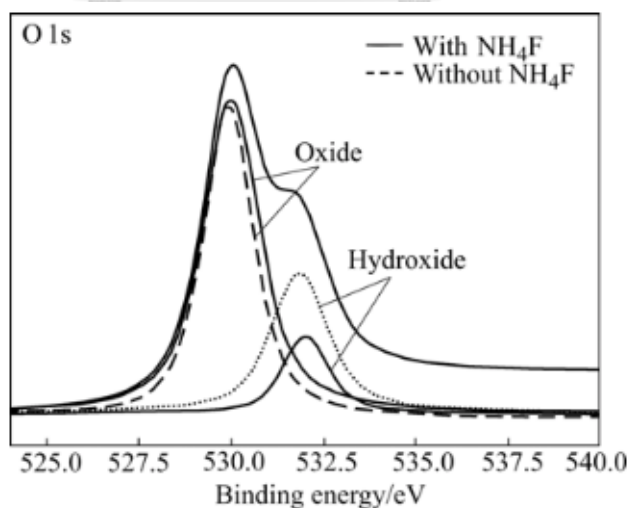


Figure 37 XPS spectra of TiO_2 nanorods that anodized at 20 V for 60 min in the different electrolytes: glycerin : D.I. water (70 : 30) with 1.5% NH_4F and without NH_4F electrolyte [22].

The XPS spectra TiO_2 nanorods, which synthesized at 20 V for 60 min in the different electrolytes: glycerin : D.I. water (70 : 30) with 1.5% NH_4F and without NH_4F electrolyte was shown in **Figure 3.19**, the binding energy of TiO_2 nanorods consists of the oxide peak at 530.1 eV and the hydroxide peak at 531.9 eV [22]. The electrolytes with 1.5% NH_4F and without NH_4F shown the oxide peak in the similar intensity, whereas the electrolyte with 1.5% NH_4F shown the hydroxide peak smaller than the electrolyte without NH_4F [22]. The fluoride ion in electrolyte solution is a substrate for $[\text{TiF}_6]^{2-}$ complex formation or dissolution reaction, which is the TiO_2 compact layer peeling reaction at electrolyte/oxide interface area [22]. Moreover, the presence of the fluoride ion in electrolyte solution is preventing the hydroxide precipitation of Ti^{4+} [22].

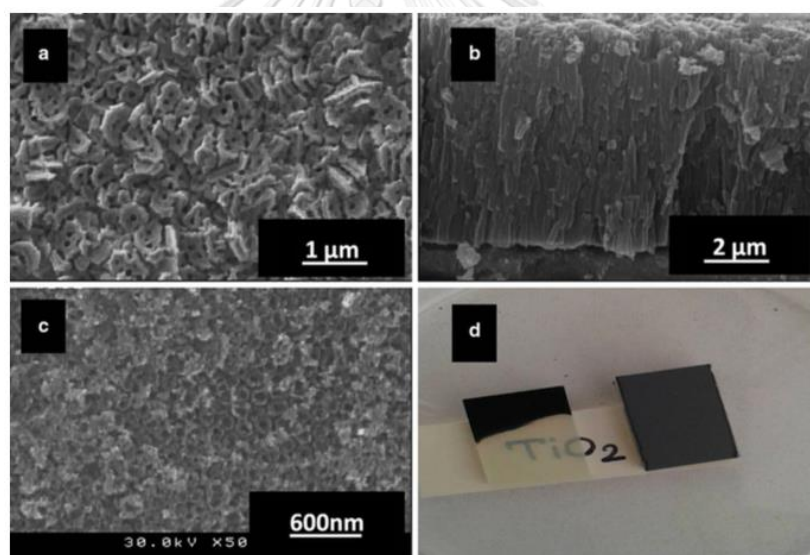
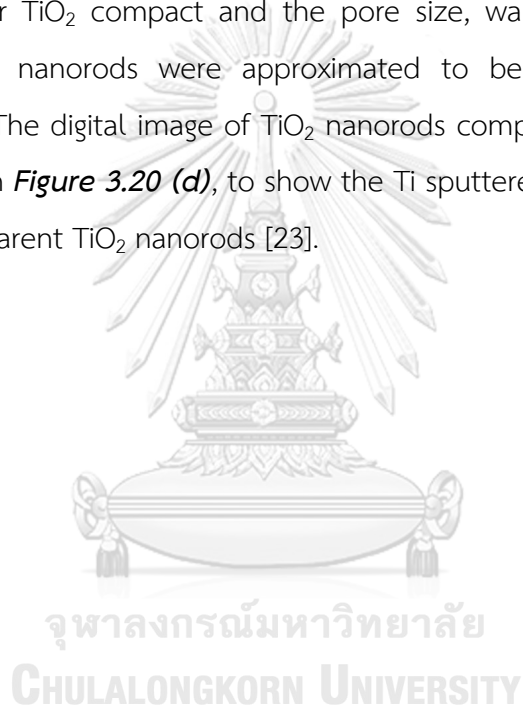


Figure 38 FE-SEM images of TiO_2 nanorods that anodized at 50 V in 0.5 wt% NH_4F and ethylene glycol electrolyte: **(a)** top view, **(b)** cross-sectional view, **(c)** bottom view, and **(d)** digital image of Ti sputtered FTO glass and the transparent TiO_2 nanorods after Ti anodization [23].

Iraj, M. (2016) has purpose electrochemical anodization of titanium in a fluoride-based electrolyte method operate with constant potential 50 V for 18 min with the electrolyte solution that was composed of 0.5 wt% of NH_4F and ethylene

glycol [23]. The Ti sputtered FTO glass substrate (thickness 2 μm of Ti layer) and stainless-steel foil were served as WE and CE, respectively, the two electrodes were set up to synthesis of the TiO_2 nanorods [23]. After that, the TiO_2 nanorods was rinsed with deionized water and ethanol to eliminate the electrolyte and then annealed at 450 $^\circ\text{C}$ for 30 min [23]. As shown in **Figure 3.20 (a)**, the top view of TiO_2 nanorods that grown on the FTO glass substrate still observe some of the TiO_2 compact on the TiO_2 nanorods [23]. The cross-sectional and bottom views of TiO_2 nanorods were shown in **Figure 3.20 (b)** and **(c)**, indicate that the TiO_2 nanorods were grown under TiO_2 compact and the pore size, wall thickness, and vectorial thickness of TiO_2 nanorods were approximated to be 70, 30, and 4,800 nm, respectively [23]. The digital image of TiO_2 nanorods compare with Ti sputtered FTO glass was shown in **Figure 3.20 (d)**, to show the Ti sputtered FTO glass was anodized into almost transparent TiO_2 nanorods [23].



CHAPTER 4

MATERIALS AND METHODS

4.1 Materials

Titanium dioxide (TiO_2) - coated fluorine-doped tin oxide (FTO) thin films was deposited on substrates glass with a working geometrical surface area of $10 \times 25 \text{ mm}^2$, a thickness of 3 mm, a thickness of $\text{TiO}_2/\text{FTO} \sim 700 \text{ nm}$ and a sheet resistance $\sim 30 \Omega/\text{sq cm}$ were supplied by Solaronix S.A.-Aubonne, Switzerland. TiO_2 on the FTO substrate is a porous TiO_2 layer that was fabricated from TiO_2 nanoparticles. TiO_2/FTO substrate glass was used as a substrate for the deposition PANI layer. The TiO_2/FTO substrates were cleaned up with detergent and rinsed with deionized water and acetone solution, respectively, in order to eliminated contaminants and impurity from the surface of the substrates. After that, the TiO_2/FTO substrates were dried in the air and then attach a transparent tape, to leave the space of the substrates away from the PANI layer, along both longitudinal sides and top $\sim 1 \text{ mm}$ on each side and $\sim 7 \text{ mm}$ below. In this research, the n-type TiO_2 was studying in two morphologies, which separate into two sets of experiments including the porous TiO_2 and the TiO_2 nanorods. Aniline ($\text{C}_6\text{H}_5\text{NH}_2$, 99.5%) was purchased from Sigma Aldrich, Singapore and hydrochloric acid (HCl, 37%) was acquired from Merck, Germany.

4.2 Synthesis of TiO_2 nanorods

The Ti sheets were cleaned up with detergent and rinsed with deionized water, acetone, and ethanol, respectively, in order to eliminated contaminants and impurity from the Ti sheet surface and then the Ti sheets were dried in the air. The electrolyte solution was composed of 0.9 wt% of NH_4F , 1.0 wt% of deionized water and ethylene glycol. Ammonium fluoride (NH_4F , >98.0%) and ethylene glycol (>=99%) were purchased from Sigma Aldrich, Singapore. The both of electrodes are a titanium sheet with a working geometrical surface area of $10 \times 25 \text{ mm}^2$, a thickness of 0.25 mm were served as the working electrode (anode) and the counter electrode (cathode), which connect to external source that is power supply at constant potential of 60 V (potentiostatic oxidation) with varying anodization times: 45 and 60

min. The overall process was happened on stirrer at 100 rpm to reduce bubble gas on the Ti sheet sample surface and the reaction was operating at room temperature that was shown in **Figure 4.1**.

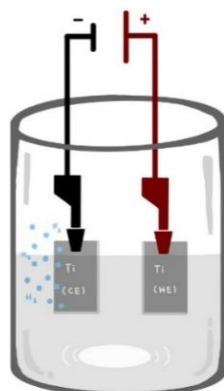


Figure 39 The synthesis of the TiO_2 nanorods by electrochemical anodization of titanium in a fluoride-based electrolyte cell.

After that, the TiO_2 nanorods sample was rinsed with deionized water to eliminate electrolyte and some of the TiO_2 compact layer that cannot peel off from the sample surface and then annealed at $500\text{ }^\circ\text{C}$ for 2 h under the heating $5\text{ }^\circ\text{C}/\text{min}$ and the natural cooling rate.

4.3 Electrodeposition of PANI on substrates

The pH reference half-cell, Ag/AgCl fill, glass body (Cole-Parmer, United States), a titanium sheet and cleaned TiO_2/FTO substrates were served as the reference electrode (RE), the counter electrode (CE) and the working electrode (WE), respectively, that was shown in **Figure 4.2**. The aqueous solution was composed of $0.5\text{ M C}_6\text{H}_5\text{NH}_2$ and 1 M HCl . The PANI layer was deposition on TiO_2/FTO substrates glass by chrono potentiometry ($\Delta t > 1\text{ ms}$) technique, which was performed by using a potentiostat (Autolab, PGSTAT101), with varying electrodeposition times: 15, 30, and 45 min at the same constant current density of 2 mA cm^{-2} and overall processes were operating at room temperature $25\text{ }^\circ\text{C}$. sputtering device (JEOL JFC-1100E) at a current of 10 mA for 30 min on the PANI/ TiO_2/FTO substrates glass which attached a masking tape.

40

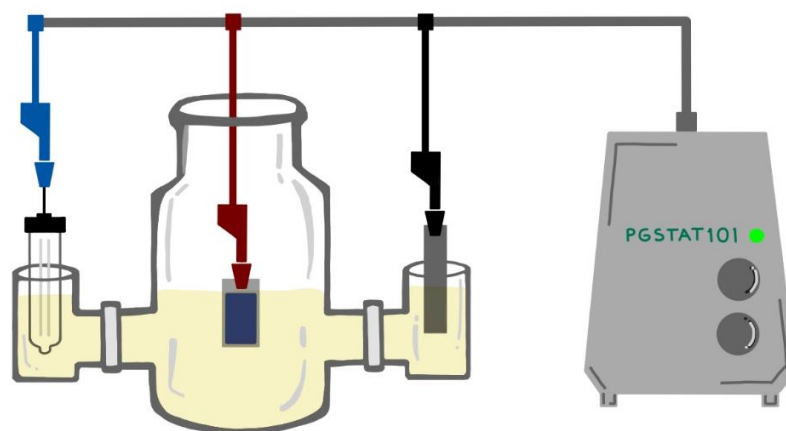


Figure 41 The glassware, RE, CE, and WE for electrochemical polymerisation of the PANI layer on the TiO_2/FTO .

The coated PANI on the TiO_2/FTO substrates glass was rinsed with deionized water to eliminate unpolymerized aniline monomer and oligomers and then the substrates were dried at room temperature. Eventually, the platinum (Pt) layer was sputtered by using an ion

4.4 Characterization and the electrochemical performances

The PANI/ TiO_2 PV cells were measured by cyclic voltammetry potentiostatic technique, which performs on a potentiostat (Autolab, PGSTAT101) with constant potential at -0.01 V and scan rate 0.05 V s^{-1} to detect I_{SC} and V_{OC} parameters of the Pt/PANI/ TiO_2 /FTO substrate in the dark and under illumination that performed under 100 mW cm^{-2} white light source (VETO ST 1000 Inc., Metal Halide & Sodium Lamp 1000W). The WE cell cable of potentiostat was clamped to the Pt layer, whereas CE and RE cell cables were connected and clamped to FTO substrates glass that shows in **Figure 4.3**. The sheet resistance (R_s) and the charge transfer resistance (R_{ct}) of PANI/ TiO_2 PV cells were measured by FRA impedance potentiostatic technique, which performs on a potentiostat (Autolab, PGSTAT302N) with constant potential at 0 V, the perturbation amplitude 10^{-2} , and frequency range were between 10^6 and 10^{-1} Hz.

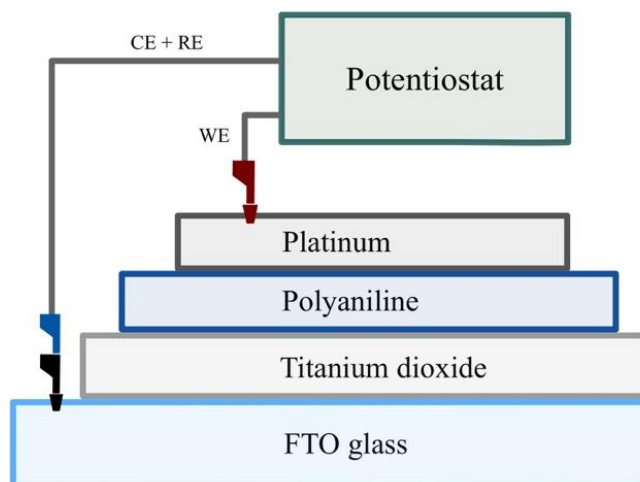


Figure 42 The cross - sectional view of the fabricated PANI/TiO₂ PV cells.

The morphology of PANI layers were characterized by Scanning Electron Microscopy (SEM) and the element in each layer of PANI/TiO₂ PV cells were analysed by Energy Dispersive X-ray Spectroscopy (EDX) and Fourier Transform Infrared Spectrophotometer (FTIR) that was determined the molecular structure of polymerized PANI on TiO₂/FTO in the wavelength of 4000 - 400 cm⁻¹. The IR spectrum of PANI that was observed in this work had many peaks that corresponding to functional groups including a peak at 1100 cm⁻¹ (Ti-O-C stretching of the interaction between carbon in PANI structure and TiO₂ layer), 1460 cm⁻¹ (C=C stretching vibration of benzenoid unit), 1560 cm⁻¹ (C=C stretching vibration of quinonoid unit), 1375 cm⁻¹ (the C-N= stretching vibration mode between benzenoid and quinoid units), 3205 - 3321 cm⁻¹ (the stretching vibration mode of the N-H bond), and 3050 - 3109 cm⁻¹ (the stretching vibration mode of aromatic C-H bond) [8, 14, 24].

CHAPTER 5

RESULTS AND DISCUSSION

5.1 Morphology

As shown in *Figure 5.1*, the thickness of TiO_2/FTO layer, it was supplied by Solaronix S.A.-Aubonne, Switzerland, was approximated to be 724 nm and the thicknesses of the deposited PANI layer with varying electrodeposition times: 15, 30, and 45 min (PANI15, PANI30, and PANI45) at the same current density of 2 mA cm^{-2} were approximated to be 301, 399, and 530 nm, respectively. The PANI thicknesses of each PANI electrodeposition time samples are an average PANI thickness that was obtained from the three PV cells.

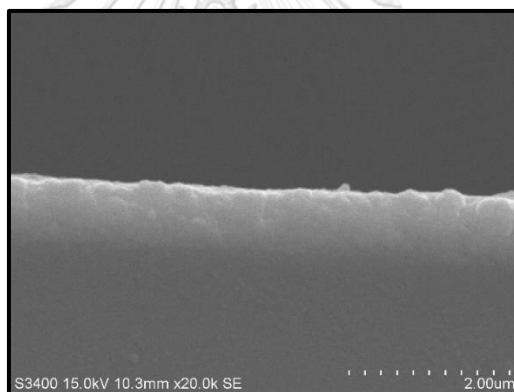


Figure 43 Cross-sectional SEM image of the TiO_2/FTO layers.

The PANI/ TiO_2/FTO layer in cross-section area with the different PANI electrodeposition times can be determined by SEM, that shows in *Figure 5.2*, *5.3*, and *5.4*. However, each layer of PV cells is difficult to observe due to the deposited PANI layer has the thickness in nanoscale. Therefore, in cracking the cell for inspection of the cross-section might also elongate the PANI layer and bring it to slightly cover the TiO_2/FTO layer. Moreover, the thickness of the TiO_2 is a porous structure that can partially absorb the deposited PANI. The porous TiO_2 cannot clearly observe by SEM and EDX but it still contained in the FTO layer and the thickness of the PANI layer in PV cell still increases in with the trend of increasing electrodeposition time.

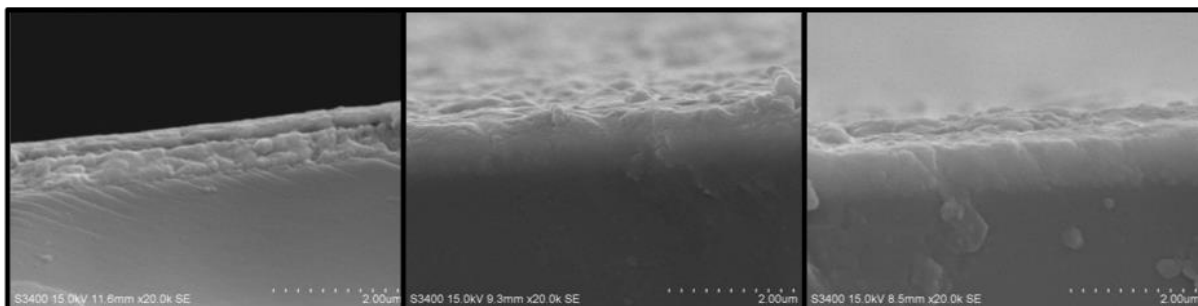


Figure 44 Cross-sectional SEM images of PANI15/TiO₂/FTO layers.

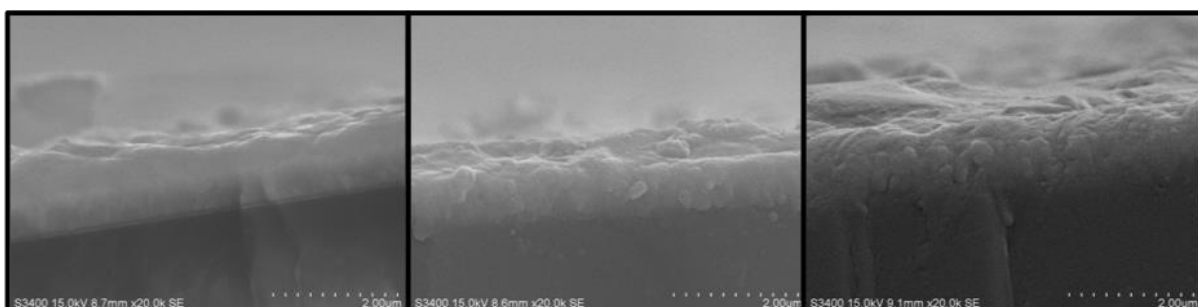


Figure 45 Cross-sectional SEM images of PANI30/TiO₂/FTO layers.

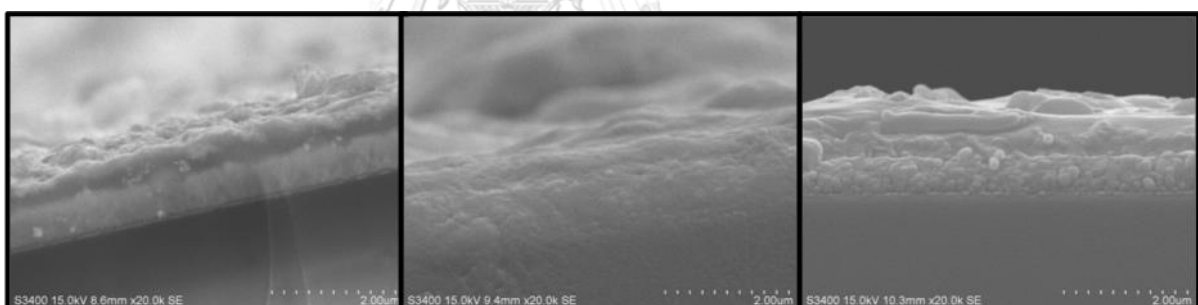


Figure 46 Cross-sectional SEM images of PANI45/TiO₂/FTO layers.

Table 5.1 Thicknesses of PANI layer with the different PANI electrodeposition times.

PANI electrodeposition times (min)	1 st cell thickness (nm)	2 nd cell thickness (nm)	3 rd cell thickness (nm)	Average thickness (nm)
15	260	339	304	301
30	434	391	373	399
45	530	513	547	530

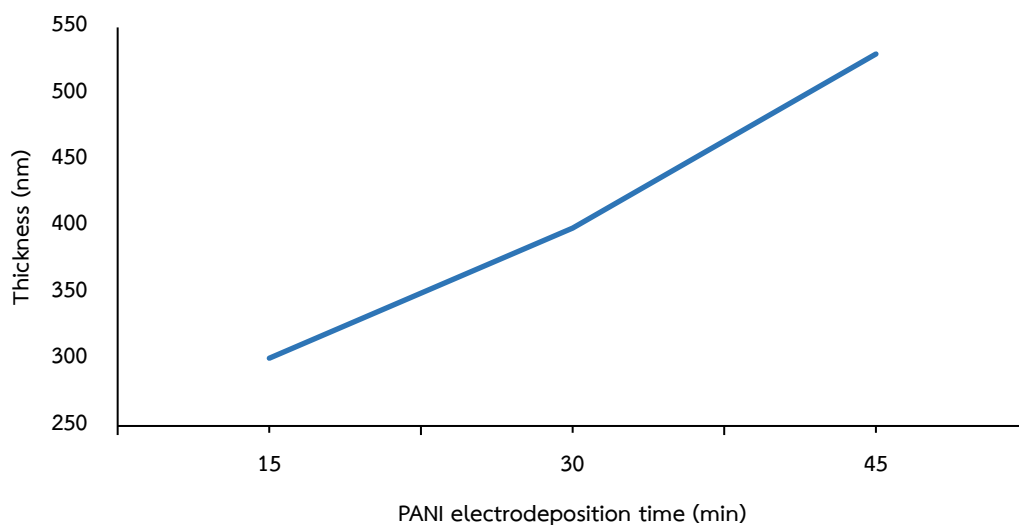


Figure 47 Calibration curve of the PANI average thicknesses with the different PANI electrodeposition times: 15, 30 and 45 min.

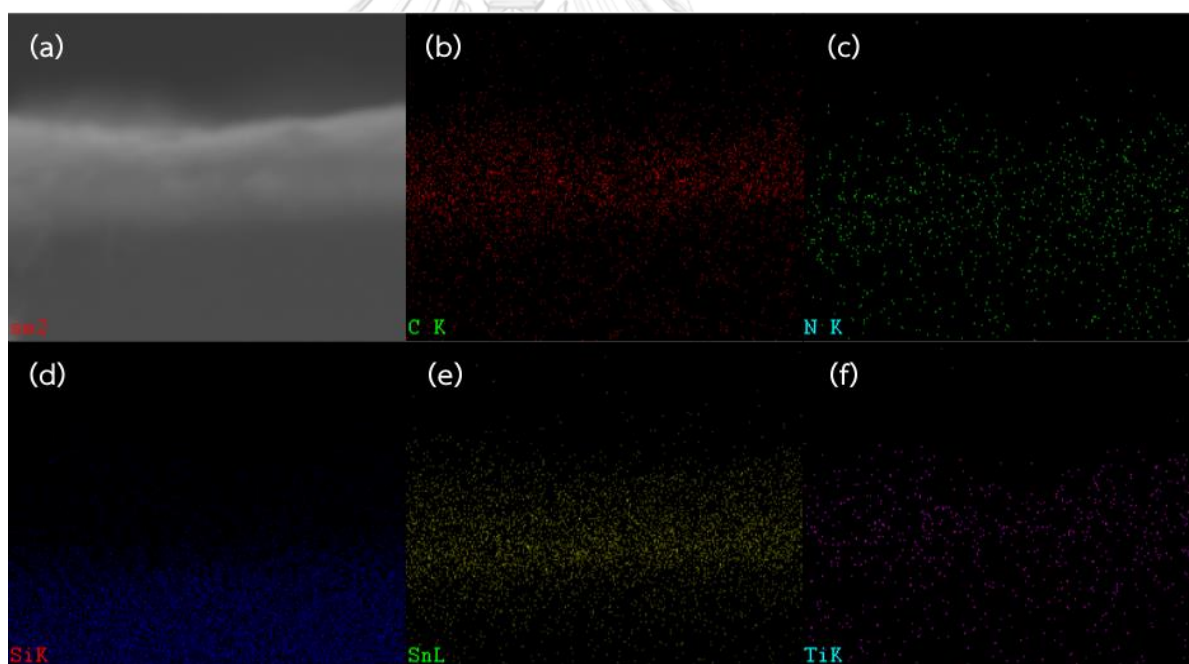


Figure 48 Cross-sectional SEM-EDX maps of the PANI45/TiO₂/FTO layers: (a) cross-sectional SEM image of PANI45/TiO₂/FTO and the elemental maps of (b) carbon, (c) nitrogen, (d) silicon, (e) tin, and (f) titanium.

The elements in each layer of the PANI45/TiO₂/FTO substrate glass were confirmed by EDX in the cross-section area. It was reported in elemental maps of

carbon, nitrogen, silicon, tin, and titanium, which appeared the carbon of the PANI45 layer was separated from the tin and silicon of the FTO layer that shows in **Figure 5.6**. The elemental maps of carbon and nitrogen of the PANI45 layer are partially distributed into the TiO₂/FTO layer due to the effect of the cross-sectional PV cell cracking step. Therefore, the elemental maps from EDX can be used as supported data for SEM images to confirm the top thickness layer in SEM image is a PANI layer that was separated on top of the TiO₂/FTO layer.

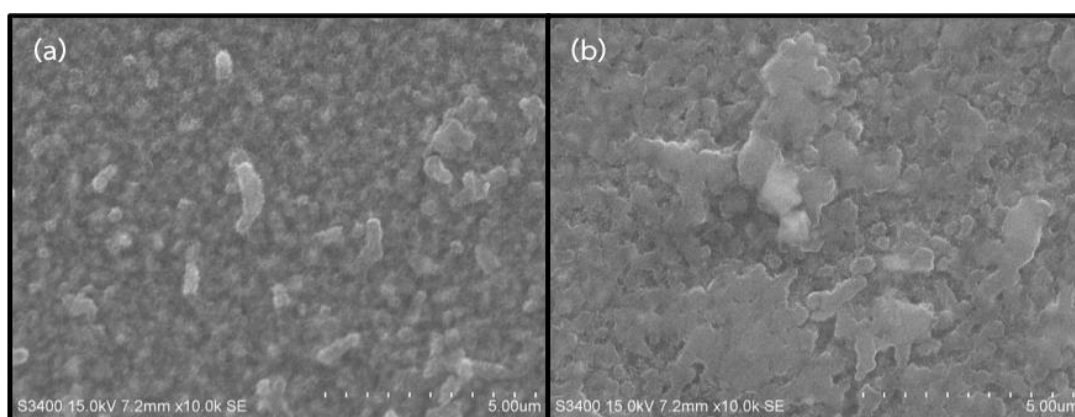


Figure 49 SEM images of PANI30 on the TiO₂/FTO substrate with the different current density of **(a)** 2 mA cm⁻² and **(b)** 5 mA cm⁻².

The effect of current density as shown in **Figure 5.7 (a)** and **(b)**, the morphology of electrodeposited PANI at the current density of 2 mA cm⁻² is a more regularly non-uniform than the morphology of electrodeposited PANI at the current density of 5 mA cm⁻², which agglomerated in non-uniform. The PANI electrodeposition at low current density is more advantageous than high current density in terms of the orderly arrangement of non-uniform polymer, the good adhesion between the deposited polymer and the substrate, the low gap between each polymer molecules, and lead to more fiber uniform. These advantages of the PANI electrodeposition at low current density were obtained from the slow electrodeposition mechanism that happened when anilinium ion was slowly adsorbed on a small partially negative charge substrate due to the low applied current density.

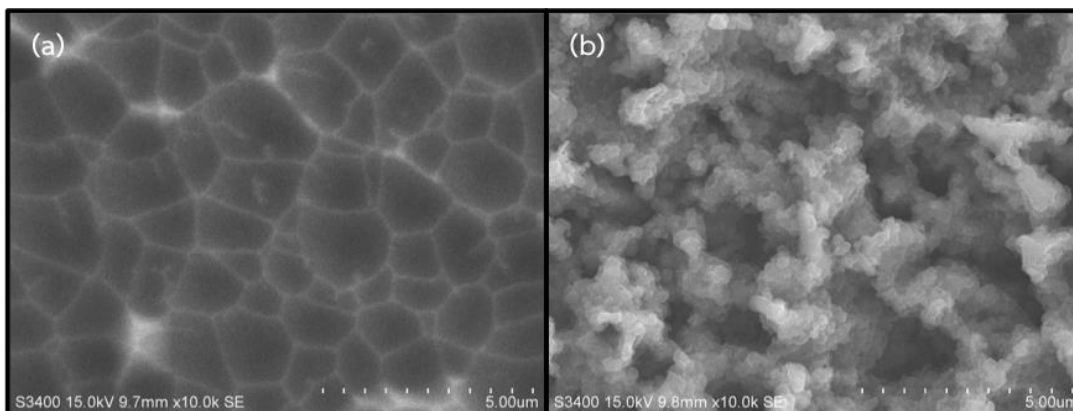


Figure 50 SEM images of the TiO_2 nanorods that anodized at 60 V in 0.9 wt% NH_4F , 1.0 wt% H_2O , and ethylene glycol electrolyte with the different anodization times: (a) 45 and (b) 60 min.

As shown in **Figure 5.8**, the TiO_2 nanorods were anodized at 60 V in 0.9 wt% NH_4F , 1.0 wt% H_2O , and ethylene glycol electrolyte with the different anodization times: 45 and 60 min (TiO_2 nanorods45 and TiO_2 nanorods60). As shown in **Figure 5.8 (a)**, SEM image of TiO_2 nanorods45 was observed the disorderly potholes morphology that is the effect of the TiO_2 nanorods formation in the second stage (ii), which is the fluoride ion in the electrolyte was penetrated through weak points on the TiO_2 compact and start to growth porous tubular layer at TiO_2/Ti interface. In addition, the second stage in TiO_2 nanorods45 formation was shift from the ideal second stage to the third stage due to the TiO_2 compact layer was peeling off, which is not balance in the tubular formation of the TiO_2 . The disorderly porous morphology of TiO_2 nanorods60 as shown in **Figure 5.8 (b)**, the TiO_2 nanorods60 formation is similar with the TiO_2 nanorods45 formation, which is the second stage that slightly shifts to the third stage but the increasing of anodization time affects to the disorderly potholes morphology was anodized into more porosity morphology, which is more surface area of the n-type TiO_2 than TiO_2 nanorods45. Many factors affect the poor tubular morphologies of TiO_2 nanorods45 and TiO_2 nanorods60 including the excess NH_4F concentration and the excess applied potential. These factors affect the formation of the TiO_2 nanorods, which can be generated by a balance between the TiO_2 formation at the oxide/metal interface and the oxide dissolution at the electrolyte/oxide interface (the TiO_2 compact layer was peeled off

in this reaction). Therefore, the NH_4F concentration was reduced from 0.9 %wt NH_4F to 0.8 %wt NH_4F with 1.0% H_2O , and ethylene glycol electrolyte to anodization of titanium at 60 V for 60 min and then the anodized TiO_2 nanorods was annealed at 500 °C. The applied potential factor was study by reduced from 60 V to 45 V to anodization of titanium with 0.9 %wt NH_4F , 1.0% H_2O , and ethylene glycol electrolyte for 60 min and then the anodized TiO_2 nanorods was annealed at 500 °C. The anodized TiO_2 nanorods with 0.8 %wt NH_4F and the anodized TiO_2 nanorods at 45 V were observed the gray layer of the TiO_2 compact cover on the blue layer of TiO_2 nanorods as shown in **Figure 5.9 (a)** and **(b)** indicate that the NH_4F concentration of 0.8 %wt and the applied potential at 45 V in this study condition is not enough for the oxide dissolution at the electrolyte/oxide interface to peeling off the TiO_2 compact layer from the TiO_2 nanorods.

Moreover, to confirm the anodization time of 60 min is the suitable anodization time for the anodization of titanium with 0.9 %wt NH_4F , 1.0% H_2O , and ethylene glycol electrolyte at a constant applied potential of 60 V. The anodization time was increased from 60 min to 75 min that was observed the corrosive Ti sheet at working electrode due to the corrosion of the dissolution reaction at the electrolyte/oxide interface as shown in **Figure 5.9 (c)**. As shown in **Figure 5.10 (a)**, **(b)**, **(c)**, and **(d)**, the SEM image of the morphologies of PANI30 on TiO_2 nanorods45 and TiO_2 nanorods60 are smaller and more orderly arrangement than PANI45 on TiO_2 nanorods45 and TiO_2 nanorods60 due to the PANI amount of PANI30 is lower than PANI45.

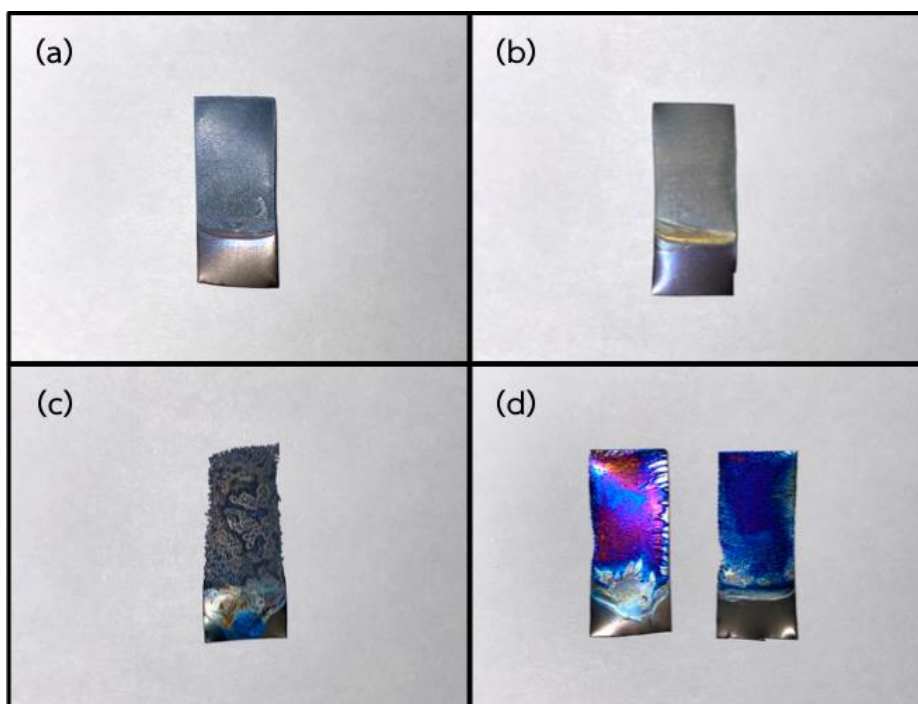


Figure 51 Digital images of (a) the anodized TiO_2 nanorods with 0.8 wt% NH_4F , (b) the anodized TiO_2 nanorods at 45 V, (c) the anodized TiO_2 nanorods at 75 min, (d) the anodized TiO_2 nanorods at 45 and 60 min.

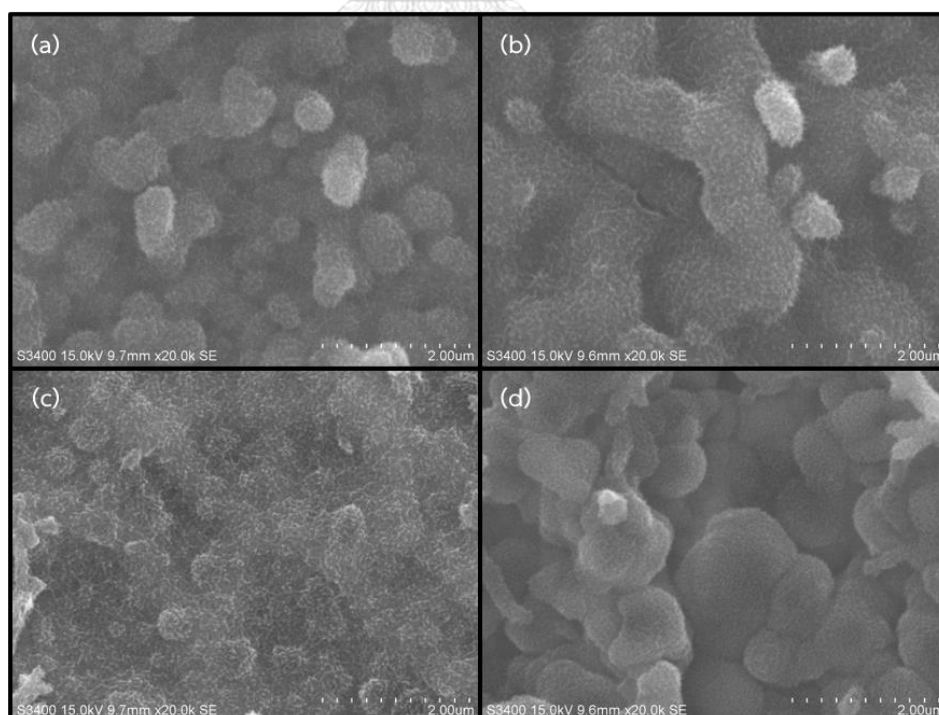


Figure 52 SEM images of TiO_2 nanorods45 that was deposited (a) PANI30 and (b) PANI45 and TiO_2 nanorods60 that was deposited (c) PANI30 and (d) PANI45.

5.2 FTIR spectra

The molecular structure of the electrodeposited PANI on the TiO₂/FTO layer will be confirmed by FTIR spectra as shown in **Figure 5.11**. The mixed two units PANI of benzenoid and quinonoid units are emeraldine oxidation state, which shows the stretching vibration mode benzenoid unit at $\sim 1460\text{ cm}^{-1}$ and quinonoid unit at $\sim 1560\text{ cm}^{-1}$ [8, 14, 24].

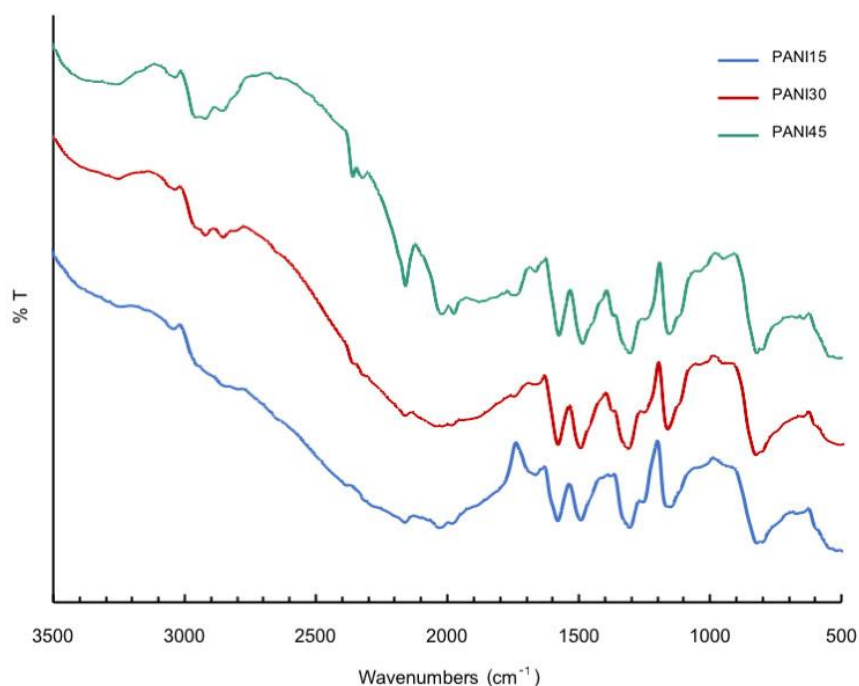


Figure 53 FTIR spectra of PANI15, PANI30, and PANI45 on TiO₂/FTO substrate glass.

Furthermore, intense peak at $\sim 1375\text{ cm}^{-1}$ in accordance with to the C=N= stretching vibration mode between benzenoid and quinoid units [8, 14, 24]. The broadband represents the stretching vibration mode of the N-H bond corresponding to the protonated nitrogen and the stretching vibration mode of aromatic C-H bond at $\sim 3205 - 3321\text{ cm}^{-1}$ and $\sim 3050 - 3109\text{ cm}^{-1}$, respectively [8, 14, 24]. The interaction between carbon in PANI structure and the TiO₂ layer was detected by the peak at $\sim 1100\text{ cm}^{-1}$, which is attributed to the Ti-O-C stretching mode [8, 14, 24]. Consequently, the oxidation state of deposited PANI is emeraldine that alternates to be a semiconductor for modified with PV cells to improve PV properties. PANI15,

PANI30, and PANI45 were shown the FTIR spectra in a similar pattern of wavenumbers indicate that the varying of electrodeposition times do not affect the oxidation state of the electrodeposited PANI.

5.3 Cyclic voltammogram

The PV behaviour of the PANI/porous TiO₂ PV cells as shown in **Figure 5.12**, the cyclic voltammogram of PANI15, PANI30, and PANI45 can be calculated the short-circuit currents (I_{sc}) by comparison at potential 0 V of the current between in the dark condition and under illumination condition: on the other hand, the open-circuit voltages (V_{oc}) can be calculated by comparison at current 0 A of the potential between in the dark condition and under illumination condition.

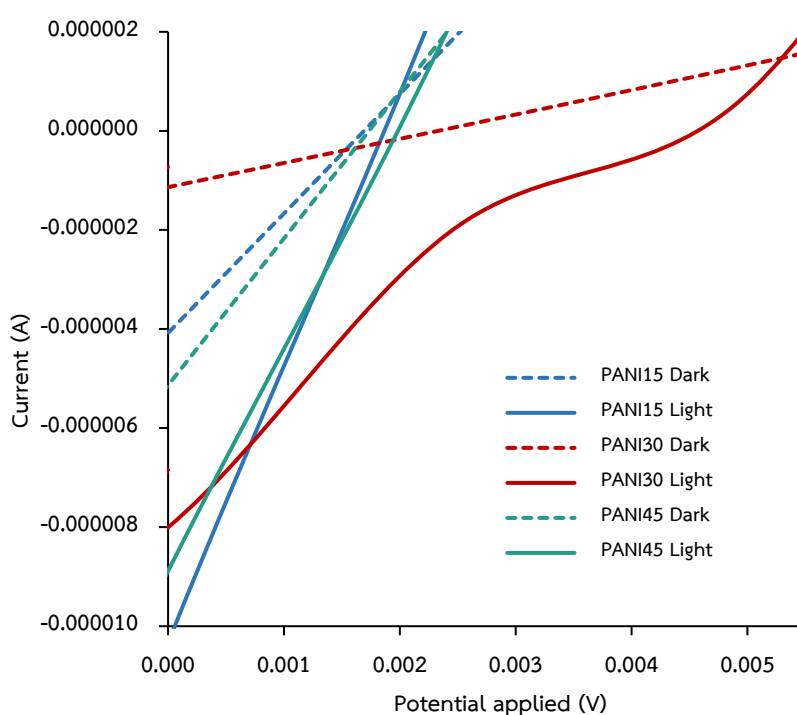


Figure 54 The overlay cyclic voltammogram of the PANI/porous TiO₂ PV cells that was deposited PANI15, PANI30, and PANI45 in the dark and under 100 mW/cm².

Table 5.2 I_{SC} and V_{OC} parameters of the PANI/porous TiO_2 PV cells that was deposited PANI15, PANI30, and PANI45 under 100 mW/cm^2 .

PANI electrodeposition times (min)	I_{SC} (μA)	V_{OC} (mV)
PANI15	6.25	0.16
PANI30	6.87	2.05
PANI45	3.75	0.23

Their parameters were reported in **Table 5.2**. As a result, I_{SC} of PANI30 (6.87 μA) is higher than PANI15 (6.25 μA) and PANI45 (3.75 μA) due to it is the optimized PANI thickness, which has a sufficient amount of PANI to conduct electricity and have appropriate resistance within the PANI/porous TiO_2 PV cells. Even though PANI15 has a thickness slightly thinner than PANI30 but PANI15 has a thickness enough to conduct electricity similar to PANI30. PANI45 has a thickness thicker than PANI30, while PANI45 has I_{SC} lower than PANI30. The small I_{SC} of PANI45 is affected by the internal resistance of PV cells caused by over PANI content, which makes charging transfer more difficult. The V_{OC} is a parameter that can identify the characteristics of PV cells. The V_{OC} of PANI15 (0.16 mV) and PANI45 (0.23 mV) are lower than PANI30 (2.05 mV), wherewith PANI15 has a low V_{OC} due to the thin thickness affecting the performance of PV cells that may cause the PANI layer can fall off from the TiO_2 layer, which is not proper for practical use. PANI45 has a low V_{OC} because of the thickness: on the other hand, PANI45 has the highest thickness. After PANI electrodeposition time at 45 min on the TiO_2 /FTO substrate, it will be rinsed with deionized water to eliminated unpolyerised aniline monomer, oligomers, and the excess PANI that not hold on the TiO_2 layer. When deionized water was rinsed on the PANI layer, the excess PANI can induce the deposited PANI on the TiO_2 layer off. Therefore, the effect of deposited PANI thicknesses affects the PV properties of PV cells.

The cyclic voltammogram of the PANI/TiO₂ nanorods PV cells with the different anodization time: 45 and 60 min, which were deposited with the different PANI electrodeposition times: 30 and 45 min as shown in **Figure 5.13** and **5.14**, the cyclic voltammogram of TiO₂ nanorods60 have the current gap between in the dark condition and under illumination condition higher than TiO₂ nanorods45 considering with the same PANI electrodeposition time indicate that the I_{SC} of TiO₂ nanorods60 is higher than TiO₂ nanorods45 due to the morphology of TiO₂ nanorods60 is more efficiency than TiO₂ nanorods45.

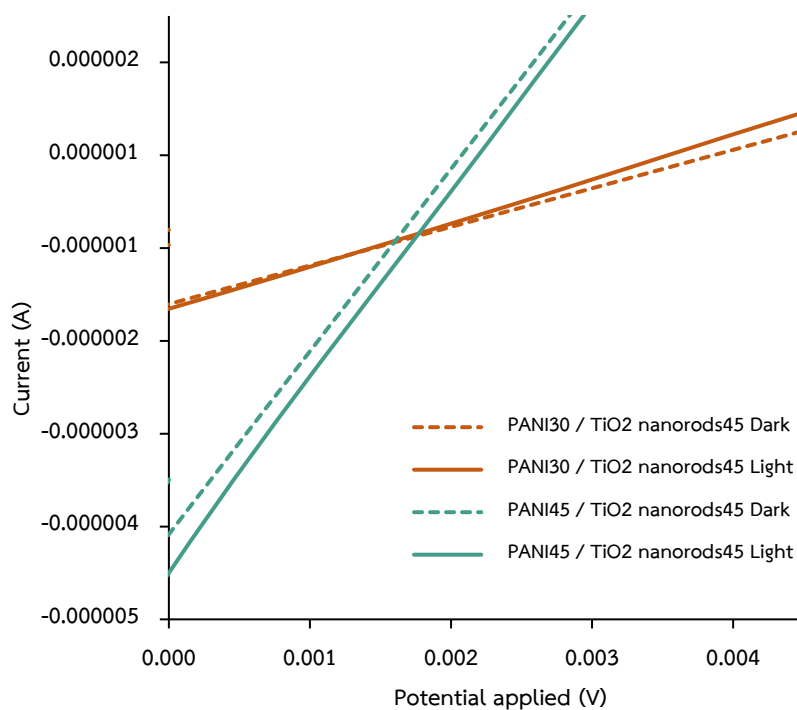


Figure 55 The overlay cyclic voltammogram of the PANI/TiO₂ nanorods45 PV cells that was deposited with PANI30 and PANI45 in the dark and under 100 mW/cm².

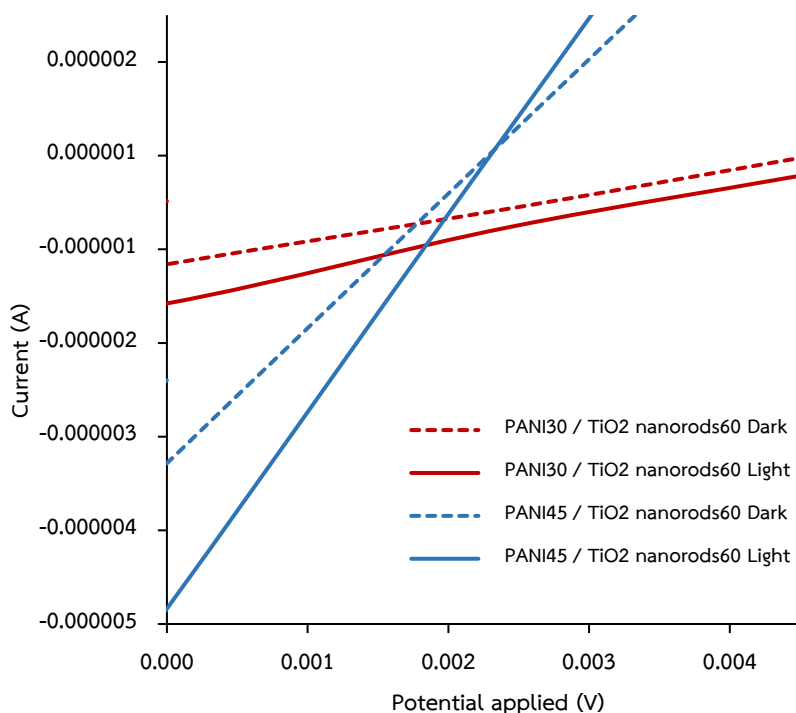


Figure 56 The overlay cyclic voltammogram of the PANI/TiO₂ nanorods60 PV cells that was deposited with PANI 30 and PANI45 in the dark and under 100 mW/cm².

Table 5.3 I_{SC} and V_{OC} parameters of the PANI/TiO₂ nanorods PV cells with the different TiO₂ nanorods anodization times that was deposited PANI30 and PANI45 under 100 mW/cm².

PANI/TiO ₂ nanorods PV cells		I_{SC} (μ A)	V_{OC} (mV)
TiO ₂ nanorods anodization times (min)	PANI electrodeposition times (min)		
45	PANI30	0.05	0.15
	PANI45	0.41	0.20
60	PANI30	0.42	0.59
	PANI45	1.55	0.13

The I_{SC} and V_{OC} parameters of the PANI/TiO₂ nanorods PV cells with the different TiO₂ nanorods anodization times and the different PANI electrodeposition times under 100 mW/cm² were reported in **Table 5.3**. Consideration in terms of the

different TiO₂ nanorods anodization times with the same PANI electrodeposition times, the I_{SC} of TiO₂ nanorods60 is always higher than TiO₂ nanorods45. Furthermore, in term of the different PANI electrodeposition times with the same TiO₂ nanorods anodization times, the I_{SC} of PANI45 is more suitable for the TiO₂ nanorods than PANI30, whereas the TiO₂/FTO substrate, which is the porous TiO₂ that was fabricated from TiO₂ nanoparticles is more efficiency when deposited with PANI30. The PANI30/TiO₂ nanorods45 have the lowest I_{SC} (0.05 μA) in the PANI/TiO₂ nanorods PV cells due to the pothole's surface of TiO₂ nanorods45 that was electrodeposition of PANI30 on their surface is poor adhesion between PANI and TiO₂ nanorods. Another factor to explain the lowest I_{SC} of PANI30/TiO₂ nanorods45 is the amount of PANI that not enough to generate proton to receive electron, which generates from the n-type TiO₂ nanorods in PV cell circuit. The I_{SC} of PANI45/TiO₂ nanorods45 (0.41 μA) is higher than PANI30/TiO₂ nanorods45 due to the amount of PANI in PANI45 is enough to work with the TiO₂ nanorods and provide the higher conductivity than PANI30 and slightly lower than PANI30/TiO₂ nanorods60 (0.42 μA) due to effect of TiO₂ nanorods60 morphology that more porosity than TiO₂ nanorods45 indicate that the PANI can deposit on TiO₂ nanorods60 surface with the good adhesion between the PANI and the TiO₂ nanorods when compare with TiO₂ nanorods45. The highest I_{SC} of the TiO₂ nanorods study is PANI45/TiO₂ nanorods60 (1.55 μA), which is a sufficient proportion between the PANI electrodeposition time and the TiO₂ nanorods anodization time. The V_{OC} of the PANI/TiO₂ nanorods PV cells are in the rage of 0.10 to 0.60 mV indicate that have an inferior adhesion between PANI and TiO₂ nanorods when compare with the PANI/porous TiO₂ PV cells.

5.4 EIS spectra

The internal resistance in the PANI/porous TiO₂ PV cells was investigated by using the electrochemical impedance spectroscopy (EIS) technique to obtain the Nyquist plots as shown in **Figure 5.15**. The internal resistance is consisting of the sheet resistance (R_s) and the charge transfer resistance (R_p or R_{ct}). The R_p in the equivalent circuit proposed to fit the Nyquist plots is the charge transfer resistance (R_{ct}) [25]. The high-frequency intercept on the real axis in the Nyquist plot is the R_s,

which corresponding to the resistance contributed by the contact resistances of the PV materials [26]. The R_{ct} is corresponding to the resistance contributed by the transfer of electrons and protons from n-type and p-type material, respectively when PV cell was absorbed photons.

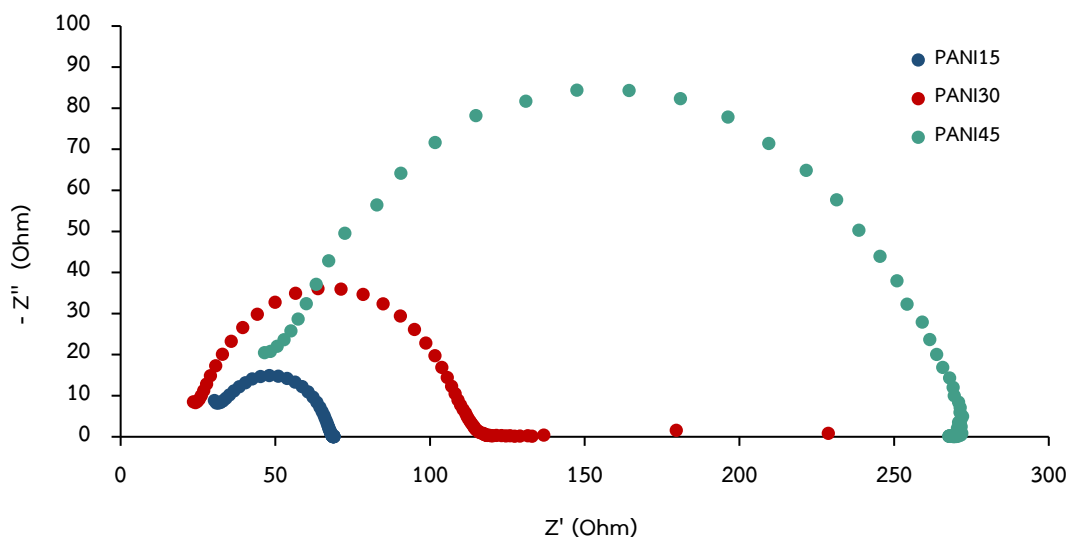


Figure 57 The overlay Nyquist plots of the PANI/porous TiO_2 PV cells that was deposited PANI15, PANI30, and PANI45.

These parameters of each PANI/ TiO_2 PV cells can be compared roughly by the diameter of the high-frequency semicircle in the Nyquist plots [26]. The R_s and R_{ct} parameters of the PANI/porous TiO_2 PV cells that was deposited PANI15, PANI30, and PANI45 were determined from the equivalent circuit proposed to fit the Nyquist plots as shown in **Figure 5.16** and the results were reported in **Table 5.4**. The R_s of the PANI/porous TiO_2 PV cells are in the range of 20.0 to 42.0 Ω . The R_{ct} is main resistance parameter that explain effect of internal resistance in the I_{SC} results. The highest R_{ct} is PANI45 (231 Ω), which is the excess amount of the PANI in the PANI/porous TiO_2 PV cells. Although PANI45 can provide many protons at the same time it more difficult protons transfer due to the high thickness of the PANI layer: on the other hand, the lowest R_{ct} is PANI15 (43.0 Ω) that corresponding to the lowest amount of the PANI that provide better protons transfer due to the thin thickness of the PANI layer but the thin PANI thickness can fall off from the TiO_2 layer, which is not proper for

practical use. Therefore, the optimized thickness of the PANI layer in the PANI/porous TiO₂ PV cells is a necessary study to obtain the optimized internal resistance that is PANI30 (101 Ω).

Table 5.4 Sheet resistance (R_s) and charge transfer resistance (R_{ct}) of the PANI/porous TiO₂ PV cells that was deposited PANI15, PANI30, and PANI45.

PANI electrodeposition times (min)	R_s (Ω)	R_{ct} (Ω)
PANI15	25.9	43.0
PANI30	20.4	101
PANI45	41.1	231

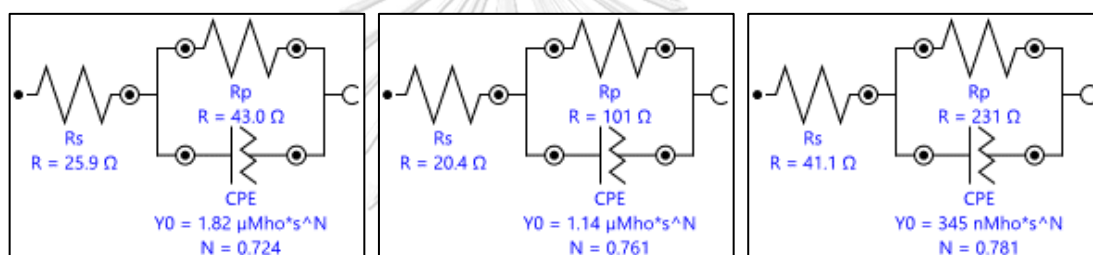


Figure 58 The equivalent circuit proposed to fit the Nyquist plots of the PANI/porous TiO₂ PV cells that was deposited PANI15, PANI30, and PANI45.

The Nyquist plots of the PANI/TiO₂ nanorods PV cells with anodization times: 45 and 60 min that were deposited PANI30 and PANI45 as shown in **Figure 5.17** and **Figure 5.18**. The R_s and R_{ct} parameters of the PANI/TiO₂ nanorods PV cells that were deposited PANI30 and PANI45 were determined from the equivalent circuit proposed to fit the Nyquist plots as shown in **Figure 5.19** and **Figure 5.20** and the results were reported in **Table 5.5**. The R_s of the PANI/TiO₂ nanorods45 are in the range of 66.0 to 93.0 Ω and the PANI/TiO₂ nanorods60 are in the range of 31.0 to 21.0 Ω, which is the characteristic resistance of PV cell. The R_{ct} of the PANI/TiO₂ nanorods45 is always higher than the PANI/TiO₂ nanorods60 indicate that the potholes morphology of the PANI/TiO₂ nanorods45 is effect to the electrons transfer and the generation of electrons due to the poor light trapping effect.

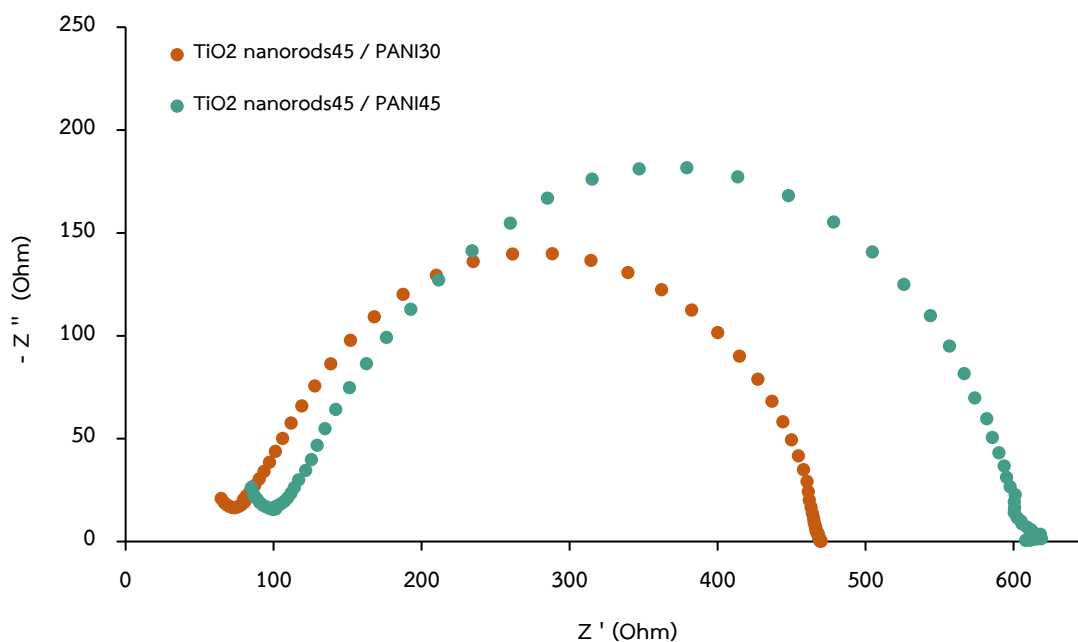


Figure 59 The overlay Nyquist plots of the PANI/ TiO_2 nanorods45 PV cells that was deposited PANI30 and PANI45.

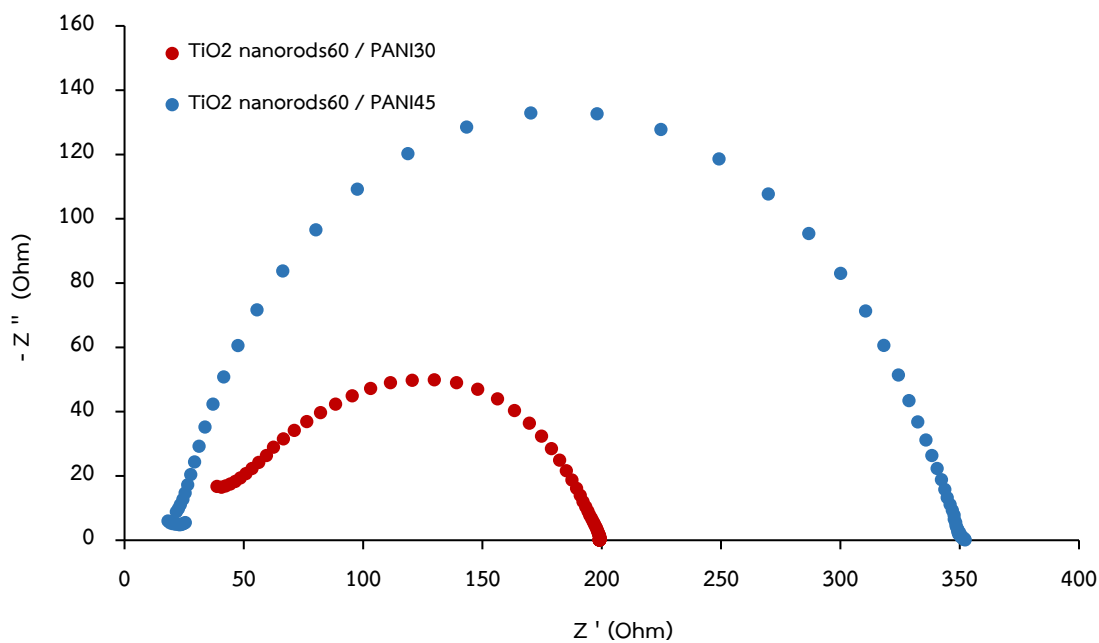


Figure 60 The overlay Nyquist plots of the PANI/ TiO_2 nanorods60 PV cells that was deposited PANI30 and PANI45.

Even though, the R_{ct} of PANI45 is always higher than PANI30 in TiO₂ nanorods45 and TiO₂ nanorods60 but does not affect the I_{sc} parameter in terms of comparison with each the PANI/TiO₂ nanorods PV cells. The internal resistance of the PANI/TiO₂ nanorods PV cells is higher than the PANI/porous TiO₂ PV cells due to the porous TiO₂ more orderly arrangement than the anodized TiO₂ nanorods in this study. The internal resistance affects to the I_{sc} parameter of the PANI/TiO₂ nanorods PV cells, which are lower than the PANI/porous TiO₂ PV cells.

Table 5.5 Sheet resistance (R_s) and charge transfer resistance (R_{ct}) of the PANI/TiO₂ nanorods PV cells with the different TiO₂ nanorods anodization times that was deposited PANI30 and PANI45.

PANI/TiO ₂ nanorods PV cells		R_s (Ω)	R_{ct} (Ω)
TiO ₂ nanorods anodization times (min)	PANI electrodeposition times (min)		
45	PANI30	66.6	418
	PANI45	92.8	529
60	PANI30	31.0	171
	PANI45	20.8	330

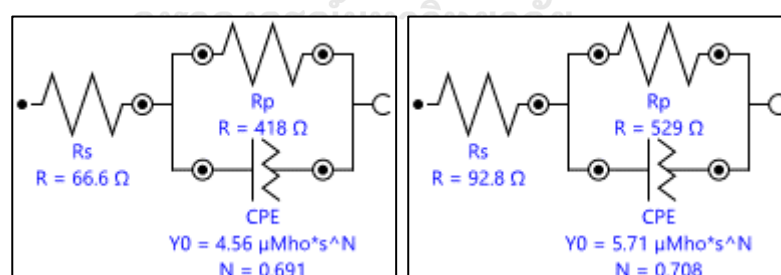


Figure 61 The equivalent circuit proposed to fit the Nyquist plots of the PANI/TiO₂ nanorods45 PV cells that was deposited PANI 30 and PANI45.

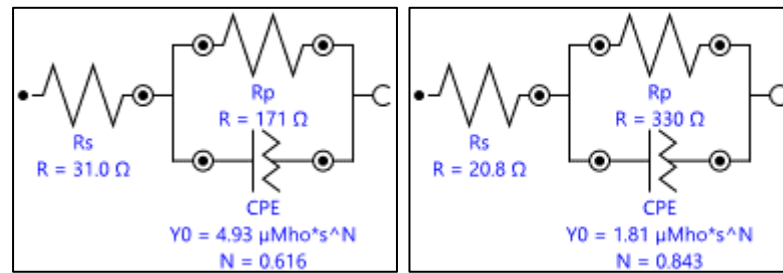


Figure 62 The equivalent circuit proposed to fit the Nyquist plots of the PANI/TiO₂ nanorods60 PV cells that was deposited PANI30 and PANI45.



CHAPTER 6

CONCLUSION AND RECOMMENDATIONS

6.1 Conclusion

Polyaniline (PANI) was synthesized directly on the porous TiO₂/FTO substrates glass by electropolymerisation, Chrono potentiometry ($\Delta t > 1$ ms) technique, at a constant current density of 2 mA cm⁻² from acidic aqueous solutions of aniline (1.0 M HCl and 0.5 M aniline) to form the PANI/TiO₂ p-n junctions with photovoltaic properties. The oxidation state of electrodeposited PANI is the emeraldine form, which is a useful state to be a potent semiconductor for PANI/TiO₂ PV cells. The optimized thickness of the PANI layer on the TiO₂/FTO substrate glass was obtained by using electrodeposition time at 30 min (PANI30) corresponding to a PANI thickness of ~ 399 nm, which showed I_{SC} (6.87 μ A) and V_{OC} (2.05 mV) higher than PANI15 and PANI45 due to the low internal resistance of PANI30. The TiO₂ nanorods were synthesized by the electrochemical anodization of titanium in a fluoride-based electrolyte (0.9 wt% of NH₄F, 1.0 wt% of H₂O, and ethylene glycol) at 60 V for 60 min is the sufficient condition for the PANI electrodeposition at 45 min (PANI45/TiO₂ nanorods60), which showed I_{SC} (1.55 μ A) higher than PANI30/TiO₂ nanorods45, PANI30/TiO₂ nanorods60, and PANI45/TiO₂ nanorods45. The porous TiO₂ is an n-type material that performs with the electrodeposited PANI better than the anodized TiO₂ nanorods in this work due to the high internal resistance of the anodized TiO₂ nanorods.

6.2 Recommendations

- 1) The electrochemical deposition of PANI on the porous TiO₂/FTO substrate glass can improve in many aspects including the varying of the PANI electrodeposition time in narrow scale between 15 min to 30 min, change the acid solution from HCl into stronger acid such as HClO₄, and change the n-type material or the morphology of TiO₂ to form the perfect p-n junction with the p-type PANI.

- 2) To improve the synthesis of the TiO_2 nanorods by electrochemical anodization of titanium in a fluoride electrolyte, the concentration of NH_4F and the applied potential should reduce in narrow range to perform the efficiency formation of the TiO_2 nanorods.



REFERENCES

1. Nemade, K., P. Dudhe, and P. Tekade, *Enhancement of photovoltaic performance of polyaniline/graphene composite-based dye-sensitized solar cells by adding TiO₂ nanoparticles*. Solid State Sciences, 2018. **83**: p. 99-106.
2. Energy.gov. *Solar Photovoltaic Cell Basics*. 2019 [cited 2019 25 Oct]; Available from: <https://www.energy.gov/eere/solar/articles/solar-photovoltaic-cell-basics>.
3. Wan, J., et al., *A facile method to produce TiO₂ nanorods for high-efficiency dye solar cells*. Journal of Power Sources, 2019. **438**.
4. Awuzie, C.I., *Conducting Polymers*. Materials Today: Proceedings, 2017. **4**(4): p. 5721-5726.
5. Matsuki, N., et al., *π -Conjugated polymer/GaN Schottky solar cells*. Solar Energy Materials and Solar Cells, 2011. **95**(1): p. 284-287.
6. Bae, S., et al., *Enhanced performance of polymer solar cells with PSSA-g-PANI/Graphene oxide composite as hole transport layer*. Solar Energy Materials and Solar Cells, 2014. **130**: p. 599-604.
7. Kerileng M., M., et al., *Electronics of Conjugated Polymers (I): Polyaniline*. International Journal of Electrochemical Science, 2012. **7**(12): p. 11859-11875.
8. Bhandari, S., *Polyaniline*, in *Polyaniline Blends, Composites, and Nanocomposites*. 2018. p. 23-60.
9. Kirk, A.P., *Energy Demand and Solar Electricity*, in *Solar Photovoltaic Cells*. 2015. p. 1-8.
10. Hernández-Callejo, L., S. Gallardo-Saavedra, and V. Alonso-Gómez, *A review of photovoltaic systems: Design, operation and maintenance*. Solar Energy, 2019. **188**: p. 426-440.
11. Jäger Klaus-Dieter, I., O., Smets, A. H. M., Swaij René A.C.M.M. van, & Zeman, M., *Solar energy: fundamentals, technology and systems*. . Cambridge: UIT Cambridge., 2016.
12. Lindholm, F.A.n.d. 1979 [cited 2020 29 Feb]; Available from: <https://www.pveducation.org/pvcdrom/solar-cell-operation/iv-curve>.

13. Seeber, R., F. Terzi, and C. Zanardi, *Intrinsically Conducting Polymers*, in *Functional Materials in Amperometric Sensing*. 2014. p. 23-57.
14. Phang, S.W., et al., *Effect of Titanium Dioxide on Adhesion and Conductivity Behavior of Polyaniline/Alkyd Composite for Solar Cell Application*. *Macromolecular Symposia*, 2018. **382**(1).
15. Tan, F., et al., *Conjugated molecule doped polyaniline films as buffer layers in organic solar cells*. *Synthetic Metals*, 2013. **178**: p. 18-21.
16. Boeva, Z.A. and V.G. Sergeyev, *Polyaniline: Synthesis, properties, and application*. *Polymer Science Series C*, 2014. **56**(1): p. 144-153.
17. Vaenas, N., T. Stergiopoulos, and P. Falaras, *Titania Nanotubes for Solar Cell Applications*, in *Electrochemically Engineered Nanoporous Materials*. 2015. p. 289-306.
18. Landmann, M., E. Rauls, and W.G. Schmidt, *The electronic structure and optical response of rutile, anatase and brookite TiO₂*. *J Phys Condens Matter*, 2012. **24**(19): p. 195503.
19. Gizzie, E.A., et al., *Photosystem I-polyaniline/TiO₂ solid-state solar cells: simple devices for biohybrid solar energy conversion*. *Energy & Environmental Science*, 2015. **8**(12): p. 3572-3576.
20. Budi, S., Ayuningsih, A., Pratiwi, C., Paristiowati, M., Fadiran, R., & Sugihartono, I., *Electropolymerization of Polyaniline Film as a Conductive Layer for the Electrodeposition of NiCo Alloy*. *Journal of Physics: Conference Series* 2020. **1428**, 012017.
21. Karami, H., M.G. Asadi, and M. Mansoori, *Pulse electropolymerization and the characterization of polyaniline nanofibers*. *Electrochimica Acta*, 2012. **61**: p. 154-164.
22. Lee, B.-G., et al., *Formation behavior of anodic TiO₂ nanotubes in fluoride containing electrolytes*. *Transactions of Nonferrous Metals Society of China*, 2009. **19**(4): p. 842-845.
23. Iraj, M., et al., *TiO₂ nanotube formation by Ti film anodization and their transport properties for dye-sensitized solar cells*. *Journal of Materials Science: Materials in Electronics*, 2016. **27**(6): p. 6496-6501.

24. Shao, W., et al., *The Effect of a Small Amount of Water on the Structure and Electrochemical Properties of Solid-State Synthesized Polyaniline*. *Materials*, 2012. **5**(10): p. 1811-1825.
25. Harrington, D.A. and P. van den Driessche, *Mechanism and equivalent circuits in electrochemical impedance spectroscopy*. *Electrochimica Acta*, 2011. **56**(23): p. 8005-8013.
26. Wu, K., et al., *Effect of Transition-Metal Ion Doping on Electrocatalytic Activities of graphene/polyaniline-M²⁺ (Mn²⁺, Co²⁺, Ni²⁺, and Cu²⁺) Composite Materials as Pt-Free Counter Electrode in Dye-Sensitized Solar Cells*. *Polymer-Plastics Technology and Materials*, 2018. **58**(1): p. 40-46.





จุฬาลงกรณ์มหาวิทยาลัย
CHULALONGKORN UNIVERSITY

VITA

NAME Akkharaphak Auisakul

DATE OF BIRTH 17 January 1996

PLACE OF BIRTH Surat Thani, Thailand

INSTITUTIONS ATTENDED B.S. (Chemistry) Faculty of Science at Kasetsart University

HOME ADDRESS 259/41 Wara-Thani Village, Pongprasart Subdistrict,
Bangsaphan District, Prachuapkhirikhan Province 77140

